Regulatory roles of 5′ UTR and ORF-internal RNAs detected by 3′ end mapping

Philip P. Adams[1,2], Gabriele Baniulyte[3], Caroline Esnault[4], Kavya Chegireddy[5], Navjot Singh[3], Molly Monge[3], Ryan K. Dale[4], Gisela Storz[1,6] and Joseph T. Wade[3,5,6]

[1]Division of Molecular and Cellular Biology, Eunice Kennedy Shriver National Institute of Child Health and Human Development, Bethesda, MD 20892-5430, USA.

[2]Postdoctoral Research Associate Program, National Institute of General Medical Sciences, National Institutes of Health, Bethesda, MD 20892-6200, USA.

[3]Wadsworth Center, New York State Department of Health, Albany, NY, USA.

[4]Bioinformatics and Scientific Programming Core, Eunice Kennedy Shriver National Institute of Child Health and Human Development, Bethesda, MD 20892-5430, USA.

[5]Department of Biomedical Sciences, School of Public Health, University at Albany, Albany, New York, USA.

[6]Corresponding Author

Email: storzg@mail.nih.gov; joseph.wade@health.ny.gov

ABSTRACT

Many bacterial genes are regulated by RNA elements in their 5′ untranslated regions (UTRs). However, the full complement of these elements is not known even in the model bacterium *Escherichia coli*. Using complementary RNA-sequencing approaches, we detected large numbers of 3′ ends in 5′ UTRs and open reading frames (ORFs), suggesting extensive regulation by premature transcription termination. We document regulation for multiple transcripts, including spermidine induction involving Rho and translation of an upstream ORF for an mRNA encoding a spermidine efflux pump. In addition to discovering novel sites of regulation, we detected short, stable RNA fragments derived from 5′ UTRs and sequences internal to ORFs. Characterization of three of these transcripts, including an RNA internal to an essential cell division gene, revealed all have independent functions as sRNA sponges. Thus, these data uncover an abundance of *cis*- and *trans*-acting RNA regulators in bacterial 5′ UTRs and internal to ORFs.

KEYWORDS: RNA-seq; Rho-dependent termination; RNA-mediated regulation; uORF; base pairing sRNAs; Hfq; ChiX; OxyS; RybB; FtsO

INTRODUCTION

The expression of many bacterial genes is controlled by elements in the 5′ untranslated regions (UTRs) of mRNAs. Changes in the secondary structures of these *cis*-acting RNA elements lead to altered expression of the associated gene(s) by modulating accessibility of ribosomes to sites of translation initiation, accessibility of RNases, or premature transcription termination. The RNA secondary structure changes can occur in response to temperature (RNA thermometers), translation of small upstream open reading frames (uORFs), or the binding of *trans*-acting factors such as metabolites (riboswitches), tRNAs, RNA-binding proteins such as CsrA, or small base pairing RNAs (sRNAs) (reviewed in (Breaker, 2018; Kreuzer and Henkin, 2018; Loh et al., 2018; Orr et al., 2020; Romeo and Babitzke, 2019; Storz et al., 2011)).

As mentioned, some of the regulatory events in 5′ UTRs are associated with premature transcription termination, which occurs by one of two mechanisms: intrinsic (Rho-independent) or Rho-dependent (reviewed in (Roberts, 2019)). Intrinsic termination requires only RNA polymerase and an RNA hairpin followed by a U-rich tract in the nascent RNA. Rho-dependent termination requires the loading of the hexameric Rho protein complex onto nascent, untranslated RNA at Rho utilization (Rut) sites that are typically C-rich, G-poor, and unstructured sequences (reviewed in (Mitra et al., 2017)). Rho translocates along the RNA until the protein catches RNA polymerase promoting transcription termination, typically between 100 and 200 nt downstream of the Rut site, leading to 3′ ends that are processed by 3′ to 5′ exonucleases (Dar and Sorek, 2018b; Wang et al., 2019).

Several studies have sought to identify sites of transcription termination across the *E. coli* genome by sequencing RNA 3′ ends or by mapping the distribution of transcribing RNA polymerase (Dar and Sorek, 2018b; Ju et al., 2019; Peters et al., 2012; Peters et al., 2009; Yan et

al., 2018). The vast majority of identified termination sites are in 3′ UTRs. In some studies, termination was compared in cells grown with/without the Rho inhibitor, bicyclomycin (BCM), facilitating the identification of Rho termination sites (Dar and Sorek, 2018b; Ju et al., 2019; Peters et al., 2012). These data provided evidence for Rho termination of mRNAs in 3′ UTRs and spurious transcripts initiated within genes. While termination within 5′ UTRs was noted in some of these studies, extensive global characterization of premature termination has not been performed. Many of the uncharacterized 3′ ends in 5′ UTRs or open reading frame (ORF)-internal regions are likely to be the result of regulatory events, given that riboswitches (Bastet et al., 2017; Hollands et al., 2012), attenuators (Ben-Zvi et al., 2019; Gall et al., 2016; Herrero del Valle et al., 2020; Konan and Yanofsky, 1997; Kriner and Groisman, 2015), RNA-binding proteins (Baniulyte et al., 2017; Figueroa-Bossi et al., 2014), and sRNAs (Bossi et al., 2012; Sedlyarova et al., 2016) have all been implicated in affecting premature Rho termination events.

In addition to being the product of a regulatory event, RNA fragments generated by premature termination or RNase cleavage themselves can have functions as regulatory sRNAs. sRNAs commonly base pair with *trans*-encoded mRNAs, frequently with the assistance of the RNA chaperone protein Hfq, resulting in changes in the stability or translation of the target mRNA (reviewed in (Hör et al., 2020)). Most sRNAs characterized to date are transcribed independent of other genes or are processed from mRNA 3′ UTRs, though a few 5′ UTR-derived sRNAs have been reported (reviewed in (Adams and Storz, 2020)). RNA fragments entirely internal to coding sequences (Dar and Sorek, 2018a) also have been suggested to function as regulators, though this has not been tested. While sRNAs generally base pair with a regulon of mRNA targets, a few small transcripts have been shown to have roles as competing endogenous RNAs (ceRNAs) also known as “sponges”, which base pair primarily with sRNAs, targeting the

sRNAs for degradation or blocking their interactions with mRNA targets (reviewed in (Denham, 2020; Figueroa-Bossi and Bossi, 2018; Grüll and Massé, 2019)).

To systematically identify new regulatory elements in *E. coli*, we globally mapped RNA 3′ ends and specifically characterized those ends in 5′ UTRs and ORF-internal regions. We compared this 3′ end dataset with another dataset where BCM treatment was used to identify Rho-dependent regions. Using these approaches, we detected hundreds of RNA 3′ ends within 5′ UTRs and internal to ORFs, likely generated by premature transcription termination or RNase processing. We propose the majority of these 3′ ends are the consequence of regulatory events, and we document regulation for multiple examples. For instance, we show 3′ ends are associated with the translation of uORFs and result from the binding of some sRNAs to mRNA 5′ UTRs. Furthermore, we demonstrate that RNA fragments generated by premature transcription termination and from within coding sequences function as independent sRNA regulators; one as part of an autoregulatory loop and another that connects cell division to the cell envelope stress response. These findings reveal extensive and diverse regulation through premature transcription termination and RNase processing of mRNAs, which can lead to the generation of RNA by-products with independent functions.

RESULTS

Global mapping of 3′ ends in *E. coli*

Two independent cultures of wild-type *E. coli* MG1655 (WT) were grown to OD_{600} ~0.4 in rich medium (LB), OD_{600} ~2.0 in LB, and OD_{600} ~0.4 in minimal (M63) glucose medium. Total RNA was isolated and analyzed using modified total RNA-seq (Shishkin et al., 2015) and 3′ end (Term-seq) protocols (Dar et al., 2016). The replicate total RNA-seq and Term-seq datasets were highly correlated (Figure S1A). Using the Term-seq data, we curated a list of dominant RNA 3′ ends (Table S1). The total numbers of identified 3′ ends were 1,175 and 882 for cells grown in LB to OD_{600} ~0.4 or 2.0, respectively, and 1,053 for cells grown in M63 glucose to OD_{600} ~0.4 (Figure S1B). The detected 3′ ends were further subclassified according to their locations relative to annotated genes (Figure 1A, Table S1). This analysis, for cells grown to OD_{600} ~0.4 in LB, revealed that, while 23% of 3′ ends mapped <50 bp downstream of an annotated gene (primary 3′ ends), hundreds of 3′ ends mapped upstream of and within ORFs (orphan and internal 3′ ends) (Figure 1B).

We compared the detected 3′ ends to those identified by three other RNA-seq based studies (Dar and Sorek, 2018b; Ju et al., 2019; Yan et al., 2018). While there was significant overlap between the 3′ ends identified in our work and those identified in each of the other studies (Figure S1C-E; hypergeometric test $p < 1e^{-100}$ in all three cases), the majority were unique to our study. Here, we focused on, and characterized, 3′ ends mapping upstream of, and internal to, coding sequences; most of these 3′ ends were not detected in the other RNA-seq studies.

Global mapping of Rho termination regions in *E. coli*

Concurrently, we mapped instances of Rho-dependent transcription termination. An *E. coli* MG1655 LB culture grown to OD_{600} ~0.5 in LB was split with half left untreated and the other half treated with 100 µg/ml BCM for 15 min. Total RNA was isolated and analyzed using a DirectRNA-seq protocol (Ozsolak and Milos, 2011), a method optimized for sequencing very short reads (20 to 30 nt) directly from RNA, an advantage for examining the effect of Rho on the generation of small RNA fragments. Using these data, we calculated a "Rho score" for each genomic position by comparing DirectRNA-seq coverage 500 nt upstream and downstream in the treated (+BCM) and untreated (-BCM) samples (see Materials and Methods). This ratio reflects the degree of transcriptional readthrough in the +BCM cells. Using a minimum threshold Rho score of 2.0, 412 genomic loci were putatively associated with a Rho termination event (Table S2). We note that these genomic positions likely correspond to processed RNA 3′ ends rather than the termination sites, since Rho-terminated transcripts typically are processed by 3′ to 5′ exonucleases (Dar and Sorek, 2018b; Wang et al., 2019). Hence, we refer to the identified genomic locations as "Rho termination regions". 14% of the Rho termination regions are <50 bp downstream of an annotated gene (primary) and are likely to reflect Rho termination events in mRNA 3′ UTRs (Figure 1C). However, as for the 3′-end mapping by Term-seq, many of the Rho termination regions were located in 5′ UTRs or within ORFs (orphan and internal 3′ ends).

The C:G nucleotide usage was calculated for the putative Rho termination regions (Table S2), as well as for a control group of randomly selected genomic coordinates. Relative to the control group, there was a higher local C:G ratio within 200 nt of the 3′ ends associated with Rho termination regions (Figure 1D), consistent with enrichment for C-rich, G-poor sequences attributed to Rut sites (reviewed in (Mitra et al., 2017)). We also compared the sites with Rho termination scores ≥ 2.0 (Table S2) to the sites of Rho termination reported in three previous

genome-wide studies (Dar and Sorek, 2018b; Ju et al., 2019; Peters et al., 2012) (Figure S1F). Again, there was significant overlap with each of the three previous studies (hypergeometric test $p < 1e^{-23}$ in all cases), though many (37%) of the putative Rho termination regions we identified are >500 bp away from any of the previously identified Rho termination regions (Dar and Sorek, 2018b; Ju et al., 2019; Peters et al., 2012).The comparison of our Term-seq LB 0.4 dataset (Table S1) with our DirectRNA-seq LB 0.5 dataset (Table S2) revealed that 239 of the 3′ ends are within Rho termination regions (Figure S1G), suggesting that these 3′ ends are associated with Rho-terminated transcripts. In general, the large sets of Rho termination regions that differ between the studies indicate that much remains to be learned about Rho-dependent termination.

Known regulatory events are associated with 3′ ends and Rho termination regions in 5′ UTRs

Many 3′ ends identified by Term-seq mapped upstream or internal to annotated mRNAs (Table S1). We specifically collated these 3′ ends (see Materials and Methods) since we hypothesized they could be reflective of regulatory events. This resulted in 3′ end lists of 665 and 507 for the LB 0.4 and LB 2.0 samples, respectively, and 580 for the M63 0.4 sample (Table S3). Among the 3′ ends in 5′ UTRs, several corresponded to sites of known *cis*-acting RNA regulation (annotated in Table S3). These include mRNAs that previously have been shown to be regulated by premature Rho-dependent termination, such as the riboswitch-regulated genes *thiM* (Bastet et al., 2017) (Figure S2A), *mgtA* (Hollands et al., 2012), *ribB* (Hollands et al., 2012) and *lysC* (Bastet et al., 2017), and the translationally-repressed genes *ilvX* (Lawther and Hatfield, 1980) and *topAI* (Baniulyte and Wade, 2019). We also noticed that even some 5′ UTRs where regulation has been reported to be at the level of translation, such as the RNA thermometer

upstream *rpoH* (Morita et al., 1999a; Morita et al., 1999b) and at ribosomal protein operons (reviewed in (Zengel and Lindahl, 1994)), harbored defined 3′ ends in 5′ UTRs.

For the LB 0.4 Term-seq dataset, for which the growth conditions were most similar to those of the DirectRNA-seq dataset, we determined a Rho score for each 3′ end (Table S3, see Materials and Methods). We also used a previously-described quantitative model to rate putative intrinsic terminators, where a score over 3.0 is predictive of intrinsic termination (Chen et al., 2013). Based on these analyses, we predict that most 3′ ends for the LB 0.4 dataset in Table S3 were formed due to RNA processing, since only 20% had secondary structures with high scores for intrinsic termination (terminator score ≥ 3.0), and 4% had a significant Rho score (≥ 2.0). However, the number of Rho termination sites is likely an underestimate because inhibition of Rho with BCM leads to extensive read-through transcription from very strongly transcribed genes, 3′ ends generated by Rho termination are typically unstable (Dar and Sorek, 2018b; Wang et al., 2019), and some 3′ends may be generated by a combination of mechanisms. However, overall, our data suggest that modulation of premature transcription termination in 5′ UTRs or ORFs is a widespread regulatory mechanism.

Novel sites of regulation are predicted by 3′ ends and Rho termination regions in 5′ UTRs

Several genes harboring Rho-dependent 3′ ends within the 5′ UTR or ORF have not been previously described as being regulated by Rho but are associated with characterized *cis*-acting RNA regulators. Examples are the *sugE* and *moaA* genes, which are preceded by the guanidine II riboswitch (Sherlock et al., 2017) and molybdenum cofactor riboswitch (Regulski et al., 2008), respectively. A browser image of the RNA-seq data for the *sugE* locus in the LB 0.4 condition highlights a predominant 3′ end 76 nt downstream the *sugE* transcription start site (TSS) (Figure

2A). This region was associated with significant readthrough in the +BCM DirectRNA-seq sample and a Rho termination score of 2.3 (Table S3), strongly suggesting that the riboswitch impacts Rho-dependent premature termination, as is the case for other riboswitches.

While the involvement of 5′ UTRs in *sugE* and *moaA* regulation was known, most of the genes for which we found 3′ ends in 5′ UTRs or ORFs have not been reported to have RNA-mediated regulation (Table S3). In some cases, such as the *mdtJI* mRNA, encoding a spermidine excretion complex, we observed a novel 3′ end that is clearly Rho-dependent (Figure 2B). In other cases, such as *ispU* (*uppS*), encoding the undecaprenyl pyrophosphate synthase, a novel 3′ end was observed with no readthrough upon Rho inhibition (Figure 2C). This 3′ end had an intrinsic termination score (Chen et al., 2013) of 14.1 (Table S3), and we predicted a six bp stem-loop followed by eight U residues, consistent with intrinsic termination.

To further test whether genes associated with 3′ ends in 5′ UTRs or ORFs are indeed regulated by premature transcription termination, we generated *lacZ* transcriptional reporter fusions using the entire 5′ UTR and ORF for representative genes with a range of calculated Rho scores from 0.8 to 2.9 (Table S3). All constructs had the same constitutive promoter. β-galactosidase activity was assayed in the context of a WT *E. coli* background or a mutant strain with an R66S substitution in Rho (*rhoR66S*), which disrupts the primary RNA-binding site (Baniulyte et al., 2017; Bastet et al., 2017; Martinez et al., 1996). A fusion to *thiM*, which harbors a 5′ UTR Rho-dependent terminator (Bastet et al., 2017), exhibited significantly higher levels of β-galactosidase activity in the Rho mutant strain, indicative of a disruption in Rho-dependent termination (Figure S2B). Northern analysis identified an RNA consistent with the 3′ end identified by Term-seq (Figure S2C), though we noted the abundance of this 5′ RNA fragment and extent of read through in the Rho R66S mutant varied with growth phase.

Among the other constructs assayed, the expression of 14 fusions was >2-fold higher in *rhoR66S* compared to WT cells (Figure 2D and S2D), consistent with Rho termination in the 5′ UTR or ORF for *sugE*, *cfa*, *cyaA*, *mdtJ*, *add, cspB, cspG, moaA, pyrG, yhaM, ydjL, yhiL, ytfL* and *yajO*. The effect of the Rho mutation on the *eptB* fusion was intermediate (1.6-fold) (Figure 2D), while the fusions to *ispU* (Figure 2D), as well as *mnmG*, *rpsJ*, *argT*, *srkA* and *trmL* (Figure S2D), displayed similar levels of β-galactosidase activity (1.0- to 1.4-fold) for *rhoR66S* compared to WT cells. These assays support the notion that the 3′ end observed in the *ispU* 5′ UTR (Figure 2C) is generated by intrinsic termination. We were surprised to find that fusions to the *ompA*, *yebO*, *glpF* and *rimP* 5′ UTR and ORF had decreased expression in the Rho mutant background (Figure S2D). This may be a consequence of additional levels of regulation or indirect effects of Rho inhibition.

Transcriptional *lacZ* reporter gene fusions to only the 5′ UTR (i.e. without the ORF) were also generated for seven genes, to distinguish between Rho termination in the ORF and in the 5′ UTR. The effect of *rhoR66S* was eliminated for the shorter *cyaA* and *eptB* fusions (Figure 2E), suggesting that Rho-dependent termination occurs within the coding sequence of these genes. Rho termination in 5′ UTRs probably is associated with the accessibility of Rut sequences, whereas Rho termination within coding sequences probably is associated with regulated translation initiation (reviewed in (Kriner et al., 2016)), with translational repression indirectly leading to Rho termination.

Finally, northern analysis was performed with probes for the 5′ UTRs of *sugE*, *cfa*, *cyaA*, *speA*, *mdtJ*, *eptB* and *ispU* using RNA extracted from WT and *rhoR66S* strains grown to OD_{600} ~0.4 and 2.0 in LB (Figure 2F). For all of the mRNAs, we detected fragments that likely correspond to the 3′ ends detected by Term-seq (indicated with an asterisk) in both growth

conditions (Table S3). For *sugE* and *cfa*, however, the dominant band on the northern blot was not necessarily the most dominant 3′ end sequenced using Term-seq. The longer transcripts for *sugE*, *cfa*, *cyaA* and *mdtJ* enriched in the *rhoR66S* samples reflect transcriptional readthrough, consistent with Rho-dependent termination as seen for the *lacZ* fusions. The effect of *rhoR66S* on *eptB* was intermediate, while no effect was observed for *ispU*. For all of the Rho-terminated genes, there was an increase in the levels of short transcripts, as seen most strikingly for *speA*. This may be explained by higher levels of longer transcripts in the absence of Rho, which are processed to give the shorter products. Additionally, the effects of the *rho* mutation varied under the different growth conditions tested, as is most obvious for *cfa* and *cyaA*. Collectively, these data validate premature termination in 5′ UTRs and, in several cases, suggest complex regulation.

Premature Rho termination of *mdtJI* is dependent on spermidine and translation of a uORF

The *mdtJI* mRNA, encoding a spermidine exporter, has a long 5′ UTR (TSS located 278 nt from the start codon) (Figure 3A) and a 3′ end that mapped 6 nt into the ORF (Figure 2B). Additionally, the transcript is subject to premature Rho termination (Figure 2D-F). The levels of the *mdtJI* transcript were previously reported to increase in response to high levels of spermidine, a polyamine (Higashi et al., 2008a), though a mechanism for this regulation was not described. Polyamines play important roles in RNA-mediated regulation, reported to cause structural changes to the 5′ UTR of the *oppA* mRNA (Higashi et al., 2008b; Yoshida et al., 1999) and induce ribosome stalling at a uORF in the 5′ UTR of the *speFL* mRNA (Ben-Zvi et al., 2019; Herrero del Valle et al., 2020). In light of these studies, we examined the effect of

spermidine on *mdtJI* mRNA levels. Total RNA was extracted from cells grown in LB medium with or without 10 mM spermidine at either neutral or high pH (spermidine and other polyamines have a stronger negative effect on cell growth at high pH (Yohannes et al., 2005)). Northern analysis of these samples probed for the *mdtJI* mRNA revealed a ~280 nt transcript, consistent with the 3′ end detected by Term-seq (Table S3), that was susceptible to readthrough upon the addition of spermidine for cells grown at high pH (Figure 3B). We therefore hypothesized that spermidine inhibits premature Rho termination of the *mdtJI* mRNA.

Closer inspection of the *mdtJI* 5′ UTR revealed a putative upstream small ORF (uORF) of 34 codons with the stop codon 106 nt upstream of the *mdtJ* AUG (Figure 3A). Translation of this uORF was previously detected by ribosome profiling, with expression of the corresponding small protein (YdgV) documented by western blot analysis (Weaver et al., 2019). To independently verify translation of the uORF, the coding sequence was translationally fused to *lacZ* together with the upstream sequence and native *mdtJI* promoter. Robust β-galactosidase activity was detected for cells carrying the fusion (Figure 3C). By contrast, no β-galactosidase activity was observed for cells carrying an equivalent fusion with the uORF start codon mutated (ATG→ACG), supporting the conclusion that the uORF (*ydgV*), here renamed *mdtU*, is indeed translated.

To investigate the role of *mdtU* in *mdtJI* spermidine-mediated regulation, the *mdtU* start codon mutation (ATG→ACG) was introduced on the chromosome of a strain where a 3XFLAG tag was translationally fused to C-terminus of MdtJ. Northern and western blot analysis of strains encoding *mdtJ-3XFLAG* showed mRNA and protein levels were strongly induced by spermidine, which was abolished in the strain with the *mdtU* start codon mutation (Figure 3D). We suggest that translation of MdtU is critical for spermidine-mediated expression of MdtJ. Northern

analysis was also carried out to determine if Rho termination in the *mdtJI* 5′ UTR impacts the induction by spermidine. In the *rhoR66S* strain, the spermidine-dependent increase in full-length *mdtJI* mRNA levels was substantially reduced relative to WT cells (Figure 3E). Together, these data support the model that spermidine, Rho and translation of the *mdtU* uORF affect the levels of MdtJI and hence spermidine transport, though the mechanisms deserve further study. A screen for uORFs upstream of *mdtJ* orthologs in other gammaproteobacterial species showed that MdtU, particularly the C-terminal region, is conserved in at least 17 genera (Figure S3). This suggests that *mdtU*-dependent regulation of *mdtJI* expression is a conserved process that may depend on the sequence of the MdtU C-terminus.

The presence of 3′ ends downstream of putative uORFs could be a way to identify new uORF-dependent regulatory sequences. A search for 3′ ends located <200 nt downstream of experimentally validated, but uncharacterized potential uORFs (Hemm et al., 2008; VanOrsdel et al., 2018; Weaver et al., 2019) revealed nine examples: *ybgV-gltA*, *yhiY-yhiI*, *ykiE-insA-7*, *yliM-ompX*, *ymdG-putP*, *ymiC-acnA*, *yqgB-speA*, and *ytgA-iptF* (Table S3), consistent with this suggestion.

5′ mRNA fragments can be generated by sRNA-mediated regulation

The vast majority of characterized regulatory binding sites for sRNAs are in 5′ UTRs, and we observed several RNA 3′ ends in 5′ UTRs near positions of documented sRNA base pairing (Table S3). For instance, the *eptB*, *ompA* and *chiP* mRNAs, which are targets of MgrR (Moon and Gottesman, 2009), MicA (Udekwu et al., 2005) and ChiX (Figueroa-Bossi et al., 2009), respectively, all had 3′ ends directly downstream of the sequences involved in sRNA base pairing (Figure 4A and Figure S4). The presence of RNA 3′ ends at these positions suggested

that stable 5′ mRNA fragments could be generated or perhaps protected by sRNA-mediated regulation. Indeed, 5′ transcripts for *eptB* and *chiP* were previously detected by total RNA-seq (Dar and Sorek, 2018a), and the *chiP* 5′ transcript was reported to accumulate in the absence of the 3′-to-5′ phosphorolytic exoribonuclease PNPase (Cameron et al., 2019).

To examine how sRNAs impacted the 5′ derived mRNA fragments of *eptB*, *ompA* and *chiP*, we used northern analysis to examine the consequences of deleting the cognate sRNA gene, or overexpressing the sRNA, on the levels of both the full-length mRNAs (Figure 4B) and 5′ fragments (Figure 4C). As expected, given the known sRNA-mediated down regulation of *eptB*, *ompA* and *chiP*, the levels of the target mRNAs were elevated in the sRNA deletion background compared to the WT strain and decreased with sRNA overexpression (Figure 4B). Some other transcripts were detected for *eptB* (~400 nt), *ompA* (<3,000 nt), and *chiP* (~200-500 nt), but these did not match the expected sizes for the mRNAs and may be degradation or readthrough products. For the 5′ UTR region of *eptB*, there was a reciprocal effect of the Δ*mgrR* background, with a strong decrease in the abundance of a ~140 nt band (Figure 4C). Given that the *eptB* 3′ end is associated with a medium Rho score (1.8, Table S3), and we observed a moderate effect of Rho mutation (Figure 2D, F), we speculate that MgrR base pairing both promotes Rho termination and protects the resultant RNA from exonucleases. For the 5′ UTR region of *ompA*, which showed the least de-repression in the Δ*micA* strain, there was a decrease in the abundance of an ~120 nt fragment in the deletion strain (Figure 4C), and the levels of this fragment increased upon MicA overexpression. These effects are consistent with MicA sRNA-directed cleavage of the *ompA* mRNA generating the fragment, or the sRNA base pairing protecting the 3′ end from exonucleolytic processing. The effect of the Δ*chiX* background on the *chiP* 5′ fragment was strikingly different. Instead of decreasing, we observed with a large

increase in the levels of an ~90 nt RNA (Figure 4C). Given the strong signal detected for this transcript, we hypothesized that this RNA may have an independent role as a regulatory RNA.

ChiZ and IspZ sRNA sponges derive from 5′ UTRs

To test the hypothesis that 5′ UTR transcripts with defined bands might have independent functions as sRNAs, we carried out further studies on the ~90 nt *chiP* 5′ UTR transcript (Figure 4C), which we renamed ChiZ, and the 81 and 60 nt *ispU* 5′ UTR transcripts (likely expressed from two TSSs with a shared 3′ end, Figure 2F), denoted IspZ (Figure S5A). Given that the binding of the sRNA ChiX to the mRNA *chiP* (containing ChiZ) increases Rho-mediated regulation of *chiP* (Bossi et al., 2012), we tested the role of Rho on ChiZ levels (Figure 5A). The effects of the *rhoR66S* mutant were dependent on growth phase, with a decrease in ChiZ for cells grown in LB to OD_{600} ~0.4, when ChiZ levels are highest. In contrast, IspZ levels were not affected by the *rhoR66S* mutant (Figure 2F), and IspZ is likely subject to intrinsic termination as stated previously.

To obtain more information about the expression of these putative sRNAs, we performed northern analysis using the same RNA analyzed in the Term-seq experiment (Figure S5B). Distinct bands were detected for the two 5′ UTRs, consistent with the generation of stable RNAs. While ChiZ was predominant in cells grown to exponential phase in LB, IspZ was abundant in LB and M63 glucose medium in both exponential and stationary phase. Since many sRNA levels are negatively affected by the lack of the RNA chaperone Hfq (reviewed in (Hör et al., 2020)), we also conducted northern analysis using RNA extracted from WT or Δ*hfq* cells across growth in LB (Figure S5B). Similar to other base pairing sRNAs and consistent with Hfq

binding, ChiZ abundance was low in the Δ*hfq* background. IspZ levels were only slightly affected by the absence of Hfq, though this region is bound by Hfq (Melamed et al., 2020).

Given their association with Hfq, we tested the independent functions of ChiZ and IspZ as base pairing sRNAs. Since the region of *chiP* encoding ChiZ has been documented to be a target for base pairing with the sRNA ChiX through compensatory mutations (Figueroa-Bossi et al., 2009; Overgaard et al., 2009), we postulated that ChiZ reciprocally regulates ChiX, sponging its base pairing activity. To test this possibility, we assayed the effects of ChiZ overexpression. As for chromosomally-encoded ChiZ (Figure S5B), longer transcripts were observed for plasmid-encoded ChiZ, likely due to readthrough, but only the levels of the 90 nt ChiZ band were strongly reduced in the Δ*hfq* mutant (Figure S6A). Upon ChiZ overexpression in the WT background, we observed increased levels of the *chiP* mRNA, without a change in ChiX levels (Figure 5B). The levels of the *chiP* mRNA overall were higher in the Δ*hfq* mutant background, but we no longer observed an increase upon ChiZ overexpression, likely due to the instability of ChiX and ChiZ. We also observed upregulation of a P_{BAD}-*chiP-lacZ* chromosomal translational fusion (Schu et al., 2015) upon ChiZ overexpression in a WT but not a Δ*chiX* background (Figure 5C). These observations support a novel sRNA regulatory network in which an mRNA (*chiP*) that is the target of an sRNA (ChiX) produces an RNA fragment (ChiZ) that reciprocally sponges the sRNA (ChiX) (Figure 5D).

We expected IspZ also might function as a base pairing sRNA, and thus searched for potential targets identified by RIL-seq (Melamed et al., 2020; Melamed et al., 2016), an approach where RNAs in proximity on an RNA binding protein are identified by co-immunoprecipitation, ligation and sequencing of the chimeras. The predominant target for IspZ in these datasets is the oxidative stress-induced sRNA OxyS (Altuvia et al., 1997). This

observation led us to test whether IspZ might act as a sponge of OxyS. As for chromosomally-encoded IspZ (Figure S5B), and in contrast to ChiZ, little readthrough and no effect of Δ*hfq* was observed for plasmid-expressed IspZ (Figure S6B). We examined the effect of IspZ overexpression on OxyS levels in cells treated with 0.2 mM hydrogen peroxide, a condition known to induce OxyS expression (Altuvia et al., 1997). High levels of IspZ were associated with slightly lower OxyS levels, in line with sponging activity (Figure 5E). To obtain evidence for direct base pairing between IspZ and OxyS, IspZ was mutated on the overexpression plasmid (IspZ-M1), and compensatory mutations were introduced into the chromosomal copy of OxyS (OxyS-M1). Consistent with the predicted pairing (Figure 5F), IspZ-mediated down-regulation was eliminated with IspZ-M1 or OxyS-M1 alone but restored when both mutations were present (Figure 5G).

Putative ORF-internal sRNAs

We also noted examples of abundant 3′ ends internal to ORFs (Table S3), downstream of nearby 5′ ends previously identified by dRNA-seq (Thomason et al., 2015), and associated with a strong signal in total RNA-seq (Figure 6). A previous study suggested that some sRNAs might be derived from sequences internal to ORFs; however, this was just inferred from total RNA-seq data (Dar and Sorek, 2018a). To test whether we could detect defined transcripts for these internal signals, we selected candidate RNAs derived from the *ftsI* (renamed FtsO), *aceK*, *rlmD*, *mglC*, and *ampG* ORFs for further investigation (Figure 6A). Analysis of dRNA-seq data (Thomason et al., 2015) suggested that the FtsO, *aceK* int and *ampG* int 5′ ends likely are generated by RNase processing of the overlapping mRNA, whereas *rlmD* int and *mglC* int likely are transcribed from promoters internal to the overlapping ORFs. In all cases, the RNA 3′ ends

are not predicted to be due to Rho-dependent transcription termination events (Rho scores < 2.0, Table S3), strongly suggesting they are generated by RNase processing or, for *aceK* int, intrinsic termination (termination score (Chen et al., 2013) = 5.9, Table S3).

Northern analysis was performed for these RNAs using the same RNA analyzed in the Term-seq experiment (Figure 6B); distinct bands were detected for all the RNAs tested. While FtsO and *ampG* int were similarly abundant in all growth conditions, *mglC* int and *rlmD* int were only expressed in cells grown in LB, and *aceK* int was most abundant in LB at OD_{600} ~2.0. We also conducted northern analysis using RNA extracted from WT or Δ*hfq* cells across growth (Figure 6B). The *aceK* int transcript was strongly dependent upon *hfq*, whereas the other RNAs were unaffected by the *hfq* deletion, though all five transcripts co-immunoprecipitate with Hfq (Melamed et al., 2020; Melamed et al., 2016). Additionally, the ORF-internal sRNAs are found in chimeras with other putative mRNA and sRNA targets in RIL-seq datasets (Melamed et al., 2020; Melamed et al., 2016): FtsO and RybB, *aceK* int and *ompF*, *rlmD* int and MicA, *mglC* int and ArcZ, *ampG* int and CyaR, suggesting these ORF-internal transcripts have independent regulatory functions.

ORF-internal FtsO is an sRNA sponge

To test for the suggested regulatory function, we focused on FtsO, which is encoded internal to the coding sequence of the essential cell division protein FtsI and exhibited high levels across growth (Figure 6B). The predominant target for FtsO in the RIL-seq datasets was the sRNA RybB (Figure 7A) followed by the sRNA CpxQ (Melamed et al., 2020). The Hfq-mediated FtsO-RybB interaction also was detected in an independent CLASH dataset (Iosub et al., 2020). We hypothesized that FtsO functions as a sponge for RybB and CpxQ, which are induced by

misfolded outer membrane proteins and inner membrane proteins, respectively, and down-regulate the corresponding classes of proteins (reviewed in (Hör et al., 2020)). This model was tested by overexpressing FtsO in WT or Δ*hfq* cells grown to exponential and/or stationary phase (150 and 360 min after subculturing). For the 360 min time point when the levels of both RybB and CpxQ are highest, a reduction was observed for both sRNAs in cells overexpressing FtsO (Figure 7B). As observed previously, the levels of RybB and CpxQ are significantly lower in the Δ*hfq* strain, though some FtsO-dependent down regulation of RybB is still detected. To test whether the effect of FtsO overexpression on RybB levels is due to a direct interaction, we mutated the site of predicted base pairing (Figure 7C) on the plasmid copy of *ftsO*. This mutation (FtsO-M3) abolished the effect of FtsO overexpression on RybB levels (Figure 7D). The repressive effect was similarly abolished by mutating the predicted site of base pairing in the chromosomal copy of *rybB* but was restored by combining the complementary mutations in *ftsO* and *rybB* (Figure 7D).

We also mutated the chromosomal copy of *ftsO* to introduce the same nucleotide substitutions, which are silent with respect to the FtsI amino acid sequence. Cells carrying these mutations were then treated with ethanol, causing outer membrane stress, which is known to induce RybB (Peschek et al., 2019). In cells with either WT or mutant FtsO, a transient increase in RybB levels was observed 5 min after ethanol addition (Figure 7E). In WT cells, RybB levels then were decreased for 30 min after ethanol treatment. By contrast, in cells with mutant *ftsO*, RybB levels again increased at 20 min following ethanol treatment. This effect was also observed in a second experiment (Figure S7A) that documented higher RybB levels up to 60 min following ethanol treatment in *ftsO-M3* cells. We also assessed the consequences of FtsO sponging RybB on the levels of the *ompC* mRNA, a verified RybB target (Johansen et al., 2006),

for the same RNA samples. In both strains, the *ompC* mRNA levels decreased after cells were treated with ethanol but for the *ftsO-M3* mutant strain there was a further decrease at the 20 min time point (Figure 7E).

The conservation of *ftsO* was examined by aligning *ftsI* orthologs across 18 species of gammaproteobacteria, revealing a striking degree of *ftsO* conservation (91% average identity) at *ftsI* wobble positions compared to the entire *ftsI* mRNA wobble positions (67% average identity) (Figure S7B). This parallels the conservation of the RybB seed sequence (Figure S7C). Collectively, our data suggest that FtsO base pairing with RybB is conserved and lowers RybB levels and activity following outer membrane stress (Figure 7F). The work demonstrates regulatory sRNAs can be derived from sequences internal to ORFs such that the same DNA sequence encodes two different functional molecules.

DISCUSSION

Widespread premature transcription termination

Through our transcriptome-wide mapping of 3′ ends and Rho-dependent termination, we uncovered extensive RNA-mediated regulation and sRNA regulators encoded by 5′ UTRs and internal to ORFs. Other studies have previously identified RNA 3′ ends and regions of Rho-dependent termination in *E. coli* (Dar and Sorek, 2018b; Ju et al., 2019; Peters et al., 2012; Yan et al., 2018). While there was considerable overlap between our work and these prior studies, there were also substantial differences. For example, reporter gene fusion data and northern analysis supported Rho termination of *sugE*, *cfa*, *cyaA*, *speA*, and *mdtJ*, of which, only *sugE* was detected in the previous genome-wide surveys (Dar and Sorek, 2018b; Ju et al., 2019; Yan et al., 2018). Some of the differences between studies can be attributed to differences in the *E. coli* strains, growth conditions, and methods used. Indeed, we previously found that small methodological differences have a large impact on the number of mapped TSSs (Thomason et al., 2015). Like any RNA-seq method, a few 3′ ends also could be due to RNA degradation during library preparation. Nevertheless, our follow-up experiments confirmed the biological relevance of several 3′ ends in 5′ UTRs and internal to ORFs. Given that strain and growth conditions used for our Term-seq and total RNA-seq match those of the previous dRNA-seq analysis (Thomason et al., 2015), in which we identified TSSs and 5′ processed ends, the combined sets represent a valuable resource for examining the *E. coli* transcriptome (see Materials and Methods for links to interactive browsers).

The majority of the 3′ ends that we identified were classified as “internal” or “orphan” 3′ ends, most of which map within 5′ UTRs or internal to ORFs and a significant number of which are predicted to be generated by premature transcription termination. This notion of widespread

premature transcription termination has been underappreciated in other studies that detected RNA 3′ ends and Rho-mediated termination. It is generally not possible to identify the exact position of Rho termination due to the post-transcriptional RNA processing. Nevertheless, our reporter assays showed that in most cases tested, Rho termination could be localized to the 5′ UTR, suggesting that modulation of Rut accessibility in 5′ UTRs could be a common mechanism of regulation.

Multiple levels of regulation at 5′ UTRs

Presuming that many premature termination events are regulatory, we documented and characterized examples of novel, diverse regulatory events for several of the 3′ ends. Undoubtedly, other unique regulatory mechanisms exist for many of the other 3′ ends. We propose that the identification of 3′ ends in 5′ UTRs and ORFs is an effective approach to discover novel regulatory elements. Classically, these regulators, such as riboswitches and attenuators, have been identified by serendipity, studies of individual genes, or searches for conserved RNA structures (reviewed in (Breaker, 2018)), but these approaches may miss these RNA elements if the function of the downstream gene is unknown or the region is not broadly conserved. Given that Term-seq is a sensitive, relatively unbiased, and genome-wide approach, it is another means of obtaining evidence for regulation in 5′ UTRs. As an example, the Term-seq data showed that transcripts from the 5′ UTR of the *E. coli* glycerol facilitator *glpF* have different 3′ ends under LB and M63 growth conditions, which could be due to uncharacterized regulation. 3′ end-mapping applied to *E. coli* grown under other conditions or using other bacterial species should lead to the characterization of many more regulators, particularly in organisms, such as the Lyme disease pathogen *Borrelia burgdorferi* (Adams et al., 2017), that

lack any known *cis*-acting RNA elements. Consistent with broad applicability, Term-seq led to the identification of known riboregulators in *Bacillus subtilis* and *Enterococcus faecalis*, and a novel attenuator in *Listeria monocytogenes* (Dar et al., 2016).

A number of 3′ ends in 5′ UTRs and ORFs were found to be associated with uORFs. Our characterization of the *mdtU* uORF suggests that regulation of premature *mdtJI* transcription termination occurs in response to ribosome stalling induced by polyamines. Two recent studies showed that the polyamine ornithine can stall ribosomes immediately upstream of the stop codon of the *speFL* uORF, affecting Rho binding and the structure of the *speFL* mRNA (Ben-Zvi et al., 2019; Herrero del Valle et al., 2020). Strikingly, conservation of MdtU is strongest at the C-terminus and overlaps a region of the *mdtU* RNA that is predicted to base pair with the *mdtJI* ribosome binding site. Thus, a mechanism similar to the one found for *speFL* may regulate *mdtJI* induction by spermidine, a hypothesis that deserves further study, together with other examples where 3′ ends are located downstream of uORFs.

We also documented three instances of 3′ ends that localized a short distance downstream of known *trans*-acting sRNA base pairing sites. These 3′ ends could be generated by endonuclease processing as a result of sRNA base pairing, or could be due to protection against exonucleases as a result of sRNA pairing. An examination of sRNA base pairing sites predicated by RIL-seq points toward other instances of this type of regulation. For example, Term-seq identified 3′ ends immediately downstream of the predicted sRNA base pairing regions for the novel mRNA-sRNA interactions *rbsD*-ArcZ, *dctA*-MgrR, and *yebO*-CyaR detected by RIL-seq chimeras (Melamed et al., 2020). In all these instances, these ends could be a result of the sRNA regulatory effect, and in some cases, may result in the formation of a new

sRNA, as we observed for ChiZ. In general, our data further illustrate the complex regulation that occurs once transcription has initiated.

Generation of sRNAs from 5′ UTRs and internal ORF sequences

Previous studies have shown that intergenic regions and mRNA 3′ UTRs are major sources of regulatory sRNAs, with a few characterized examples of sRNAs derived from 5′ UTRs, and no characterized ORF-internal sRNAs (reviewed in (Adams and Storz, 2020)). Our data document that 5′ UTRs and ORFs can indeed encode functional base pairing sRNAs. However, our work also raises important questions, including the mechanisms by which 5′ UTR-derived and ORF-internal sRNAs are generated.

Given that sRNAs derived from 5′ UTRs only require the generation of a new 3′ RNA end (likely sharing a TSS with their cognate mRNA), and are not usually constrained by codon sequences, they could evolve rapidly. We documented the formation of several 5′ UTR fragments by *cis*-regulatory events. These by-products of regulation could obtain independent regulatory functions, as has been reported for a few riboswitches and attenuators (DebRoy et al., 2014; Melior et al., 2019; Mellin et al., 2014). The sRNA 3′ end can be formed by intrinsic termination or Rho-dependent termination and/or processing. Importantly, for the downstream mRNA to be expressed, there needs to be some transcriptional readthrough. RNA structure predictions strongly suggest the IspZ 3′ end is generated by intrinsic termination (Table S3) for which we observed very little readthrough. In contrast, the ChiZ 3′ end is generated by Rho-dependent termination with significant readthrough that would allow *chiP* expression. The mechanisms that drive formation of either 5′-derived sRNAs or the corresponding full-length mRNAs could be regulated and are an interesting topic for future work.

Less is known about both the 5′ and 3′ ends of the ORF-internal sRNAs. The ends might be generated by ORF-internal promoters, termination, or RNase processing. In cases where both sRNA ends are generated by processing, this is presumably coupled with down-regulation of the overlapping mRNA. Strikingly, the number of sequencing reads for FtsO are orders of magnitude higher than those for the *ftsI* mRNA. How and when FtsO is produced are interesting questions for future work. It is possible that the *ftsI* mRNA is protected from cleavage by ribosomes during cell division such that FtsO is only generated in the absence of mRNA translation. Other coding sequence-derived sRNAs, such as the putative regulator internal to *mglC*, likely have their own TSS. In some cases, such as *rlmD* int and *ampG* int, a transcript originating from a TSS internal to the cognate mRNA could be processed to form the 5′ end of the sRNA. These observations underscore how the interplay of transcription initiation, transcription termination, and RNase processing leads to many short transcripts that have the potential to evolve independent regulatory functions.

Roles of 5′ UTR-derived and ORF-internal sRNAs

We identified and characterized three sRNA sponges, which had 3′ ends in either 5′ UTRs or internal to the coding sequence. The first example, ChiZ-ChiX-*chiP*, represents a novel reciprocal autoregulatory loop. ChiZ is generated from the *chiP* 5′ UTR encompassing the site of pairing with the ChiX sRNA. We found ChiZ is formed by Rho-dependent termination and in the absence of ChiX base pairing with *chiP*. When cells utilize chitobiose as a carbon source and ChiX levels are naturally low, there are higher levels of *chiP* (Overgaard et al., 2009) and likely also higher levels of ChiZ. In this model, when chitooligosaccharides need to be imported, ChiZ prevents ChiX from base pairing but does not promote degradation of this sRNA. When

metabolic needs shift, ChiX could be released from ChiZ allowing ChiX to regulate *chiP* and other targets. This may work in competition, conjunction, or at separate times from the *chbBC* intergenic mRNA sequence, which also sponges ChiX, but results in ChiX decay (Overgaard et al., 2009). It will be interesting to see if other 5′ UTRs and sRNAs form similar autoregulatory loops since 5′ UTRs are enriched for sRNA pairing sites, and we have shown that sRNA pairing can lead to the generation of distinct small transcripts from 5′ UTRs.

In a second example, we characterized IspZ, which is generated from the 5′ UTR of *ispU* (*uppS*), encoding the synthase for undecaprenyl pyrophosphate (UPP), a lipid carrier for bacterial cell wall carbohydrates (Apfel et al., 1999). We suggest IspZ may connect cell wall remodeling with the oxidative stress response. Cellular levels of toxic reactive oxygen species are increased when cell wall synthesis is blocked, and oxidative damage impedes *ispU*-related cell wall growth (Kawai et al., 2015). Thus, IspZ downregulation of the hydrogen peroxide-induced sRNA OxyS may dampen the oxidative response at a time when the response might be detrimental.

While small transcripts from within coding sequences have been noted previously (Dar and Sorek, 2018a; Reppas et al., 2006), and a homolog of FtsO (STnc475) has been detected for *Salmonella enterica* (Smirnov et al., 2016), we are the first to document a regulatory role for a bacterial ORF-internal sRNA. FtsO was found to base pair with and negatively regulate the membrane stress response sRNA, RybB. The *ftsI* mRNA encodes a low abundance but essential penicillin-binding protein that is localized to the inner membrane at the division site and cell pole (Weiss et al., 1997). The cell may need to alter its response to membrane stress during the division cycle when many membrane components are needed. FtsO could facilitate crosstalk between cell division and membrane stress by regulating RybB activity. Intriguingly, we observed the greatest effect of ethanol addition on RybB levels in the Δ*ftsO* background at 20

min, which is also the doubling time for *E. coli* MG1655. While it is reasonable to assume that regulatory sRNAs encoded by intragenic sequences are rare, due to the challenge of encoding two functions in one region of DNA, we think it is likely that other ORF-internal sRNAs have function.

Our work has significantly increased the number of sRNAs documented to modulate the activities of other sRNAs by sponging their activities, as found for ChiZ, or affecting their levels, as shown for IspZ and FtsO. The findings raise other questions including how many more short transcripts generated by termination or processing have regulatory functions. It also is intriguing that some abundant sRNAs are subject to regulation by multiple sponges, including ChiX, which is regulated by ChiZ and the *chbBC* intergenic region (Overgaard et al., 2009), and RybB, which is regulated by FtsO, RbsZ (Melamed et al., 2020) and the 3´ETS^{leuZ} tRNA fragment (Lalaouna et al., 2015). Finally, little is known about how the activities and levels of the sponges themselves are regulated. The levels of some, but not others, are influenced by Hfq binding. A number appear to be constitutively expressed, such that target sRNA levels must increase to overcome the effects of the sponges.

Further identification and characterization of RNA fragments generated by premature termination or processing, detected by mapping the 5´ and 3´ ends of bacterial transcriptomes, will help elucidate the effects of regulatory RNAs. Our datasets point to a plethora of potential *cis*- and *trans*-acting regulatory elements in 5´ UTRs and ORF-internal regions, providing a valuable resource for further studies of gene regulation.

MATERIALS AND METHODS

Bacterial strains and plasmids

Derivatives of *E. coli* K12 MG1655 (WT) were used for all experimental studies. All strains, plasmids and oligonucleotides used are listed in Supplementary Table S4. Engineered mutations and plasmid inserts were verified by sequencing.

The *E. coli* strains carrying *mdtJ*-3XFLAG were engineered using the FRUIT method (Stringer et al., 2012). Briefly, a 3XFLAG-*thyA*-3XFLAG tag/selection marker was PCR-amplified with primers JW9000 + JW9001 and recombineered into strain AMD061 and then counter-selected for *thyA* loss due to recombination of the FLAG tags, resulting in the intermediate strain YY18. This intermediate was used to create the *mdtU* start codon mutant (ATG→ACG) by recombineering the PCR amplified *thyA* marker (using primers JW10309 + JW10310) into the *mdtU* gene and then replacing the *thyA* marker with the *mdtU* mutation (recombineering a PCR amplified product using primers JW10311 - JW10314). The native *thyA* locus was restored as described previously (Stringer et al., 2012).This resulted in the wild-type *mdtU mdtJ*-3XFLAG (YY20) or the *mdtU* start codon (ATG→ACG) mutant *mdtJ*-3XFLAG (AMD742) strains. The Δ*mgrR*::kan (GSO769), Δ*micA*::kan (GSO157), and Δ*chiX*::kan (GSO169) deletions (Hobbs et al., 2010) were transduced into MG1655 (GSO982) by P1 transduction, resulting in GSO993, GSO994 and GSO995 respectively. The *oxyS*-M1::kan (GSO996) and *rybB*-M3::kan (GSO997) strains were constructed by PCR amplifying the kan^R sequence in pKD4 (Datsenko and Wanner, 2000) using primers PA313 + PA314 (*oxyS*-M1) or PA218 + PA219 (rybB-M3) and recombineering the product (Datsenko and Wanner, 2000; Yu et al., 2000) into the chromosome of *E. coli* NM400 (kind gift of Nadim Majdalani). The *ftsO*-M3::kan (GSO999) strain was constructed by first transforming a temperature sensitive *ftsI*

Y380D mutant (PA215) (Dai et al., 1993), with pKD46 (Datsenko and Wanner, 2000). This strain was electroporated with an *ftsO*-M3 PCR product (amplified from the *ftsO*-M3 geneblock (Table S4) with primers PA216 + PA217) in the presence of 20 mM L-arabinose to induce the λ recombinase on pKD46. Colonies were selected by plating at 45˚C. Colony PCRs (using primers PA216 + PA217) and sequencing was performed to check for repair of the *ftsI* Y380D mutation and simultaneous *ftsO*-M3 incorporation (GSO999). A colony without the *ftsO*-M3 change was kept as a wild-type control (GSO998). All sRNA mutant alleles were subsequently transferred into *E. coli* MG1655 (GSO982) by P1 transduction.

The pMM1 β-galactosidase transcriptional reporter fusion plasmid was constructed by PCR amplifying the high expression promoter KAB-TTTG (Burr et al., 2000) from pJTW064 (Stringer et al., 2014) using primers JW10252 + JW102253, and the DNA was ligated into pAMD-BA-lacZ plasmid (Stringer et al., 2014) digested with the NsiI and HindIII restriction enzymes. Either the entire 5′ UTR and annotated ORF region or 5′ UTR region alone for selected genes was PCR amplified using the oligonucleotides listed in Table S4 and cloned into the pMM1 vector, cut with NsiI and NheI restriction enzymes, using the NEBuilder HiFi kit (NEB). The *mdtU-lacZ* translational fusions were constructed by PCR amplifying the *mdtU* gene from either a WT (*E. coli* MG1655) genomic template or *mdtU* start codon mutant (ATG→ACG) template (AMD742) using primers JW7269 + JW8934. These PCR products were subsequently ligated into the pAMD-BA-lacZ plasmid (Stringer et al., 2014), cut with SphI and HindIII restriction enzymes, using the NEBuilder HiFi kit (NEB).

sRNAs were over expressed using the pBRplac plasmid (Guillier and Gottesman, 2006). sRNA sequences were PCR amplified using the oligonucleotides listed in Table S4, digested with AatII and EcoRI, and cloned into pBRplac digested with the same restriction enzymes. The

ChiZ overexpression construct was engineered using the NEBuilder kit (NEB), according to the manufacturer's instructions with primers PA311 + PA312 and LW043 + LW044 and the pBRplac-*lacI* derivative, pNM46 (kind gift of Nadim Majdalani).

Growth conditions

Bacterial strains standardly were grown with shaking at 250 rpm at 37˚C in either LB rich medium or M63 minimal medium supplemented with 0.2% glucose and 0.001% vitamin B1. Ampicillin (100 µg/ml), kanamycin (30 µg/ml), chloramphenicol (30 µg/ml) and/or IPTG (1 mM) were added where appropriate. Unless indicated otherwise, overnight cultures were diluted to an OD_{600} of 0.05 and grown to the indicated OD_{600} or time point.

RNA isolation

E. coli cells corresponding to the equivalent of 10 OD_{600} were collected by centrifugation, washed once with 1X PBS (1.54 M NaCl, 10.6 mM KH_2PO_4, 56.0 mM Na_2HPO_4, pH 7.4) and pellets snap frozen in liquid N_2. RNA was isolated using TRIzol (Thermo Fisher Scientific) exactly as described previously (Melamed et al., 2020). RNA was resuspended in 20-50 µl DEPC H_2O and quantified using a NanoDrop (Thermo Fisher Scientific).

Term-seq

Two biological replicates of *E. coli* MG1655 (GSO988) were diluted 1:500 from an LB overnight culture in either LB or M63 glucose media. Cells were collected at an OD_{600} ~0.4 and 2.0 for LB and an OD_{600} ~0.4 for M63 grown cultures. RNA was extracted as described above and analyzed using an Agilent 4200 TapeStation System to check the quality. Any contaminating

DNA in the samples was removed by treating 15 µg of RNA with 10 U of DNase I (Roche) for 15 min at 37˚C in the presence of 80 U of recombinant RNase inhibitor (Takara Bio). Next, RNA was purified by mixing the sample with an equal volume of phenol stabilized:chloroform:isoamyl alcohol (25:24:1) and centrifugation at maximum speed in Heavy Phase Lock Gel tubes (5 PRIME). A volume of chloroform, equal to the original sample volume, was added to the same Heavy Phase Lock Gel tubes and spun again. The aqueous layer was removed and ethanol precipitated in the presence of 15 µg GlycoBlue (Ambion). RNA pellets were reconstituted in 10 µl DEPC H_2O and analyzed using an Agilent 4200 TapeStation System to ensure DNase-treated RNA was at high quality. Term-seq libraries were prepared using a modified version of the RNAtag-seq methodology (Shishkin et al., 2015), based on the previously published Term-seq methodology (Dar et al., 2016). 1.5 µg of DNA-free RNA was first ligated at the 3′ end with 150 µM barcoded oligonucleotide adapters which were 5′phosphorylated and dideoxycytidine 3′ terminated (Table S4). RNA and 3′ adapters were incubated at 22˚C for 2.5 hr with 51 U of T4 RNA Ligase I (NEB) and 12 U of recombinant RNase inhibitor (Takara Bio) in 1X T4 RNA Ligase Buffer (NEB), 9% DMSO, 20% PEG 8000, and 1 mM ATP. 3′ ligated RNA was cleaned by incubating with 2.5X volume of RNAClean XP beads (Beckman Coulter) and 1.5X volume of isopropanol for 15 min, before separation on a magnetic rack. Bead-bound RNA was washed with 80% ethanol, air dried, and resuspended in DEPC H_2O. RNA-containing-supernatants were removed and the same RNAClean XP bead cleanup protocol was repeated, with a final DEPC H_2O elution of 9.5 µl. RNA was fragmented by incubating 9 µl of cleaned-up RNA with 1X Fragmentation Reagent (Invitrogen) for 2 min at 72˚C, followed by an addition of 1X Stop Solution (Invitrogen). Samples were stored on ice following individual fragmentation of each sample. Fragmented-RNA was pooled together and

cleaned using the RNA Clean and Concentrator-5 kit (Zymo) according to the manufacturer's instructions. Library construction continued following the bacterial-sRNA adapted, RNAtag-seq methodology starting at the rRNA removal step (Melamed et al., 2018). Term-seq RNA libraries were analyzed on a Qubit 3 Fluorometer (Thermo Fisher Scientific) and an Agilent 4200 TapeStation System prior to paired-end sequencing using the HiSeq 2500 system (Illumina).

Identification of 3´ ends from Term-seq

Raw sequence reads were processed using lcdb-wf (lcdb.github.io/lcdb-wf/) according to the following steps. Raw sequence reads were trimmed with cutadapt 1.18 (Martin, 2011) to remove any adapters while performing light quality trimming with parameters "-a AGATCGGAAGAGC -q 20 –minimum-length=25." Sequencing library quality was assessed with fastqc v0.11.8 with default parameters. The presence of common sequencing contaminants was evaluated with fastq_screen v0.11.3 with parameters "–subset 100000 –aligner bowtie2." Trimmed reads were mapped to the *E. coli* reference genome (GCF_000005845.2_ASM584v2) using BWA-MEM. Multimapping reads were filtered using samtools (Li et al., 2009). Uniquely aligned reads were then mapped to gene features using subread featureCounts v1.6.2 with default parameters. BedGraph files were generated using deepTools (Ramírez et al., 2016) on reads from each strand separately.

An initial set of termination peaks was called per sample on the uniquely aligned reads using a novel signal processing approach combined with a statistically-informed method of combining multiple replicates. Briefly, the scipy.signal Python package was used to call peaks on each replicate in a manner which handled high, sharp peaks as found in Term-seq data, using the scipy.signal.find_peaks function with a width of (1, None), a prominence of (None, None), and a

relative height of 0.75. Peaks for each replicate were then combined using the IDR framework (Landt et al., 2012) into a set of peaks that were reproducible across replicates. The code for this can be found at https://github.com/NICHD-BSPC/termseq-peaks and can be used in general for Term-seq peak-calling in other bacteria. Termination peaks were subsequently curated according to the following criteria. The single-bp peak coordinate was set to the strongest signal nucleotide within the boundary of the initial broader peak using multiBigWigSummary from deepTools 3.1.3. The most downstream position, relative to the peak orientation, was chosen when several positions were equally strong. Scores from peaks within a distance of up to 100 bp were assessed to select the peak with the highest score among the cluster for further analysis. These curated peaks were used for all analysis herein (Table S1).

Total RNA-seq

Total RNA-seq was performed using the same RNA that was used for the Term-seq library preparations. Total RNA-seq library construction was carried out based on the RNAtag-seq methodology (Shishkin et al., 2015), which was adapted to capture bacterial sRNAs (Melamed et al., 2018). Total RNA-seq RNA libraries were sequenced as for Term-seq. Total RNA-seq data processing followed the same procedures as Term-seq data analysis for QC, adaptor removal and sequencing read mapping.

BCM Treatment and DirectRNA-seq

One culture of *E. coli* MG1655 cells (GSO989) was grown in LB to an OD_{600} ~0.5 and the culture was split and half was treated with 100 µg/ml of bicyclomycin for 15 min. Total RNA was isolated from 1.5 ml of untreated and BCM-treated cultures using the hot-phenol RNA extraction method followed by ethanol precipitation as described previously (Stringer et al.,

2014). Genomic DNA was removed by treating 8 μg of total RNA with 4 U of Turbo DNase (Invitrogen) for 45 min at 37˚C. DNA-free RNA was purified using phenol:chloroform:isoamyl alcohol and ethanol precipitation as described previously (Stringer et al., 2014). rRNA was removed using Ribo-Zero (Bacteria) Kit (Epicentre) according to the manufacturer's instructions. The RNA libraries were prepared and processed at the Helicos BioSciences facility where poly-A tails and a 3´-dATP block were added to make the RNA suitable for direct sequencing on the HeliScope™ Single Molecule Sequencer (Ozsolak and Milos, 2011).

Identification of Rho-dependent 3´ ends

DirectRNA-sequencing reads from untreated and BCM treated samples were aligned to the MG1655 NC_000913.3 genome using CLC Genomics Workbench, ignoring the quality scores which are not generated by the HeliScope™ Sequencer. The read count and position of sequenced transcript 3´ ends were used for further analysis. The approximate Rho-dependent transcription termination sites were predicted by identifying the locations of transcriptional readthrough in the BCM treated sample. The ratio of the read count in a 500 nt region upstream (BCM_us) and downstream (BCM_ds) of each position was compared to the same ratios at the same position in the untreated sample (Untreated_us, Untreated_ds) ($R_{(BCM/untreated)} = \frac{BCM_ds/BCM_us}{Untreated_ds/Untreated_us}$). Positions with <50 reads in a 500 nt window upstream or downstream were omitted. The ratio $R_{(BCM/Untreated)}$ threshold for termination sites was set to ≥2.0. Only the position with the highest $R_{(BCM/Untreated)}$ value within a 500 nt window upstream and downstream was reported in Table S2. A window size of 500 nt was selected as large enough to have sufficient number of reads for most regions and small enough to identify one Rho-termination

site per transcriptional unit. Note that Rho scores listed in Table S3 represent $R_{(BCM/Untreated)}$ that were calculated for specific positions matching the dominant Term-seq 3′ ends.

Classification of 3′ ends

The intersect function of Bedtools 2.28.0 (Quinlan and Hall, 2010), ran via pybedtools v0.8.0 (Dale et al., 2011), was used to assign each peak to one or more classes: Primary (3′ peaks located on the same strand either within 50 bp downstream of the 3′ end of an annotated mRNA ORF, tRNA, rRNA or sRNA with the highest score), Antisense (3′ peaks located on the opposite strand of an annotated mRNA ORF, tRNA, rRNA or sRNA within 50 bp of its start and end coordinates), Internal (3′ peaks located on the same strand within an annotated mRNA ORF, tRNA, rRNA or sRNA coordinates, excluding the 3′ end coordinate) and Orphan (3′ peak not falling in any of the previous classes).

3′ ends were also categorized according to their position relative to mRNA 5′ UTRs and internal mRNA regions (Table S3). Any 3′ end (Table S1) that was located within a region of 200 bp upstream of an annotated start codon to the stop codon were extracted and further analyzed. To remove any 3′ ends that likely belonged to an upstream gene in the same direction, TSS data (Thomason et al., 2015) obtained using the same growth conditions and *E. coli* strain as Term-seq was considered. All these 3′ ends were examined for the first upstream feature (either a TSS or an ORF stop codon). Any 3′ end where the first upstream feature was a stop codon was eliminated, unless there was also a TSS ≤ 200 bp upstream the 3′ end or that upstream feature was the stop codon of an annotated "leader peptide" on the EcoCyc *E. coli* database (*mgtL*, *speFL*, *hisL*, *ivbL*, *ilvL*, *idlP*, *leuL*, *pheL*, *pheM*, *pyrL*, *rhoL*, *rseD*, *thrL*, *tnaC*, *trpL*, *uof*). Any 3′ end where a TSS was only 20 bp or less upstream was also eliminated. This resulted in the 3′ end

coordinates in Table S3. For the LB 0.4 condition, 3′ ends were given a Rho score from Direct-RNA-seq (as described above) and an intrinsic termination score (with a custom script as defined in (Chen et al., 2013)). uORFs for which synthesis was detected by western analysis and/or translational reporter fusions (Hemm et al., 2008; VanOrsdel et al., 2018; Weaver et al., 2019), sRNAs for which synthesis was detected by northern analysis (this study) and other characterized RNA regulators were noted for the LB 0.4 condition.

β-galactosidase assays

Rho transcriptional and MdtU translational reporter assays were done as previously described (Baniulyte et al., 2017). Briefly, the pMM1constructs (Table S4) were assayed in MG1655Δ*lacZ* (AMD054) and MG1655Δ*lacZ rhoR66S* (GB4) background. Three separate colonies were grown overnight in LB with 30 μg/ml chloramphenicol, diluted 1:100 in the same medium and grown to a final OD_{600} ~0.4-0.6 at 37˚C. Cells were lysed in Z buffer (0.06 M Na_2HPO_4, 0.04 M NaH_2PO_4, 0.01 M KCl, 0.001 M $MgSO_4$), supplemented with β-mercaptoethanol (50 mM final concentration), sodium dodecyl sulfate (0.001% final concentration), and chloroform. Assays were initiated by adding 2-nitrophenyl β-D-galactopyranoside and stopped by adding Na_2CO_3. All assays were done at room temperature. The OD_{600} and A_{420} of the cultures were measured using a Jenway 6305 spectrophotometer. The translational *chiP-lacZ* fusions (PA258 and PA259) were assayed as above, with the following changes. Three separate colonies were grown overnight in LB with 100 μg/ml ampicillin, diluted to an OD_{600} of 0.05 in the same medium supplemented with 0.2% arabinose and 1 mM IPTG, and grown for 150 min (OD_{600} ~1.5) at 37˚C. Reactions were performed at 28˚C and the OD_{600} and A_{420} of the cultures were measured

using an Ultrospec 3300 *pro* spectrophotometer (Amersham Biosciences). For all experiments, β-galactosidase activity was calculated as $(1000 \times A_{420})/(OD_{600} \times V_{ml} \times time_{min})$.

Northern blot analysis

Northern blots were performed using total RNA exactly as described previously (Melamed et al., 2020). For small RNAs, 5 µg of RNA were fractionated on 8% polyacrylamide urea gels containing 6 M urea (1:4 mix of Ureagel Complete to Ureagel-8 (National Diagnostics) with 0.08% ammonium persulfate) and transferred to a Zeta-Probe GT membrane (Bio-Rad). For longer RNAs, 10 µg of RNA were fractionated on a 2% NuSieve 3:1 agarose (Lonza), 1X MOPS, 2% formaldehyde gel and transferred to a Zeta-Probe GT membrane (Bio-Rad) via capillary action overnight. For both types of blots, the RNA was crosslinked to the membranes by UV irradiation. RiboRuler High Range and Low Range RNA ladders (Thermo Fisher Scientific) were marked by UV-shadowing. Membranes were blocked in ULTRAhyb-Oligo Hybridization Buffer (Ambion) and hybridized with 5′ ^{32}P-end labeled oligonucleotides probes (listed in Table S4). After an overnight incubation, the membranes were rinsed with 2X SSC/0.1% SDS and 0.2X SSC/0.1% SDS prior to exposure on film. Blots were stripped by two 7-min incubations in boiling 0.2% SDS followed by two 7-min incubations in boiling water.

Immunoblot analysis

Immunoblot analysis was performed as described previously with minor changes (Zhang et al., 2002). Samples were separated on a Mini-PROTEAN TGX 5%–20% Tris-Glycine gel (Bio-Rad) and transferred to a nitrocellulose membrane (Thermo Fisher Scientific). Membranes were blocked in 1X TBST containing 5% milk, probed with a 1:2,000 dilution of monoclonal α-

FLAG-HRP (Sigma) and developed with SuperSignal West Pico PLUS Chemiluminescent Substrate (Thermo Fisher Scientific) on a Bio-Rad ChemiDoc MP Imaging System.

Data and Code Availability

The raw sequencing data reported in this paper have been deposited in SRA under accession number PRJNA640168. Code for calling 3′ ends in Term-seq sequencing reads can be found at https://github.com/NICHD-BSPC/termseq-peaks.

The processed RNA-seq data from this study are available online via UCSC genome browser at the following links:

E. coli Term-seq:
https://genome.ucsc.edu/cgi-bin/hgTracks?hubUrl=https://hpc.nih.gov/~NICHD-core0/storz/trackhubs/ecoli_all_Feb2019/hub.hub.txt&hgS_loadUrlName=https://hpc.nih.gov/~NICHD-core0/storz/trackhubs/ecoli_all_Feb2019/session.txt&hgS_doLoadUrl=submit

E. coli Rho-dependent 3′ ends (Term-seq LB 0.4 and DirectRNA-seq):
https://genome.ucsc.edu/cgi-bin/hgTracks?hubUrl=https://hpc.nih.gov/~NICHD-core0/storz/trackhubs/ecoli_rho/hub.hub.txt&hgS_loadUrlName=https://hpc.nih.gov/~NICHD-core0/storz/trackhubs/ecoli_rho/session.txt&hgS_doLoadUrl=submit

ACKNOWLEDGMENTS

Thank you to S. Melamed, A. Zhang, H. Zhang, L. Walling and T. Updegrove for experimental and technical assistance as well as to K. Papenfort, T. Updegrove and members of the Storz lab for helpful comments on the manuscript. P.P.A. was supported by a Postdoctoral Research Associate (PRAT) fellowship from the National Institute of General Medical Sciences (NIGMS), award number 1Fi2GM133345-01. Research in the Storz laboratory and the Bioinformatics and Scientific Programming Core was funded by the Intramural Research Program of the National Institutes of Health, *Eunice Kennedy Shriver* National Institute of Child Health and Human

Development. Research in the Wade laboratory was funded by National Institutes of Health Director's New Innovator Award 1DP2OD007188.

AUTHOR CONTRIBUTIONS

P.P.A., G.S., and J.W. conceived the project. P.P.A., G.S., G.B., and J.W. designed and analyzed the experiments. P.P.A generated the Term-seq and total RNA-seq libraries and performed all RNA-based experiments. N.S. prepared samples for DirectRNA-seq. G.B., M.M., K.C., and P.P.A. performed the β-galactosidase assays. C.E., R.D., G.B., and J.W. performed the bioinformatic analyses. P.P.A., G.S., G.B., J.W., C.E., and R.D. prepared the figures and wrote the manuscript. All authors approved the final manuscript. G.S. and J.W. supervised the project.

REFERENCES

Adams, P.P., Flores Avile, C., Popitsch, N., Bilusic, I., Schroeder, R., Lybecker, M., and Jewett, M.W. (2017). In vivo expression technology and 5' end mapping of the *Borrelia burgdorferi* transcriptome identify novel RNAs expressed during mammalian infection. Nucleic Acids Res *45*, 775-792.

Adams, P.P., and Storz, G. (2020). Prevalence of small base-pairing RNAs derived from diverse genomic loci. Biochim Biophys Acta Gene Regul Mech *1863*, 194524.

Altuvia, S., Weinsterin-Fischer, D., Zhang, A., Postow, L., and Storz, G. (1997). A small, stable RNA induced by oxidative stress: Role as a pleiotropic regulator and antimutator. Cell *90*, 43-53.

Apfel, C.M., Takács, B., Fountoulakis, M., Stieger, M., and Keck, W. (1999). Use of genomics to identify bacterial undecaprenyl pyrophosphate synthetase: cloning, expression, and characterization of the essential *uppS* gene. J Bacteriol *181*, 483-492.

Baniulyte, G., Singh, N., Benoit, C., Johnson, R., Ferguson, R., Paramo, M., Stringer, A.M., Scott, A., Lapierre, P., and Wade, J.T. (2017). Identification of regulatory targets for the bacterial Nus factor complex. Nat Commun *8*, 2027.

Baniulyte, G., and Wade, J.T. (2019). An antibiotic-sensing leader peptide regulates translation and premature Rho-dependent transcription termination of the *topAI* gene in *Escherichia coli.* bioRxiv, 682021–682021.

Bastet, L., Chauvier, A., Singh, N., Lussier, A., Lamontagne, A.M., Prévost, K., Massé, E., Wade, J.T., and Lafontaine, D.A. (2017). Translational control and Rho-dependent transcription termination are intimately linked in riboswitch regulation. Nucleic Acids Res *45*, 7474-7486.

Ben-Zvi, T., Pushkarev, A., Seri, H., Elgrably-Weiss, M., Papenfort, K., and Altuvia, S. (2019). mRNA dynamics and alternative conformations adopted under low and high arginine concentrations control polyamine biosynthesis in *Salmonella*. PLoS Genet *15*, e1007646.

Bossi, L., Schwartz, A., Guillemardet, B., Boudvillain, M., and Figueroa-Bossi, N. (2012). A role for Rho-dependent polarity in gene regulation by a noncoding small RNA. Genes Dev *26*, 1864-1873.

Breaker, R.R. (2018). Riboswitches and translation control. Cold Spring Harb Perspect Biol *10*, a032797.

Burr, T., Mitchell, J., Kolb, A., Minchin, S., and Busby, S. (2000). DNA sequence elements located immediately upstream of the -10 hexamer in *Escherichia coli* promoters: a systematic study. Nucleic Acids Res *28*, 1864-1870.

Cameron, T.A., Matz, L.M., Sinha, D., and De Lay, N.R. (2019). Polynucleotide phosphorylase promotes the stability and function of Hfq-binding sRNAs by degrading target mRNA-derived fragments. Nucleic Acids Res *47*, 8821-8837.

Chen, Y.-J., Liu, P., Nielsen, A.A.K., Brophy, J.A.N., Clancy, K., Peterson, T., and Voigt, C.A. (2013). Characterization of 582 natural and synthetic terminators and quantification of their design constraints. Nat Methods *10*, 659-664.

Dai, K., Xu, Y., and Lutkenhaus, J. (1993). Cloning and characterization of *ftsN*, an essential cell division gene in *Escherichia coli* isolated as a multicopy suppressor of *ftsA12*(Ts). J Bacteriol *175*, 3790-3797.

Dale, R.K., Pedersen, B.S., and Quinlan, A.R. (2011). Pybedtools: a flexible Python library for manipulating genomic datasets and annotations. Bioinformatics *27*, 3423-3424.

Dar, D., Shamir, M., Mellin, J.R., Koutero, M., Stern-Ginossar, N., Cossart, P., and Sorek, R. (2016). Term-seq reveals abundant ribo-regulation of antibiotics resistance in bacteria. Science *352*, aad9822.

Dar, D., and Sorek, R. (2018a). Bacterial noncoding RNAs excised from within protein-coding transcripts. mBio *9*, e01730-01718.

Dar, D., and Sorek, R. (2018b). High-resolution RNA 3'-ends mapping of bacterial Rho-dependent transcripts. Nucleic Acids Res *46*, 6797-6805.

Datsenko, K.A., and Wanner, B.L. (2000). One-step inactivation of chromosomal genes in *Escherichia coli* K-12 using PCR products. Proc Natl Acad Sci USA *97*, 6640-6645.

DebRoy, S., Gebbie, M., Ramesh, A., Goodson, J.R., Cruz, M.R., van Hoof, A., Winkler, W.C., and Garsin, D.A. (2014). Riboswitches. A riboswitch-containing sRNA controls gene expression by sequestration of a response regulator. Science *345*, 937-940.

Denham, E.L. (2020). The Sponge RNAs of bacteria - How to find them and their role in regulating the post-transcriptional network. Biochim Biophys Acta Gene Regul Mech *1863*, 194565.

Figueroa-Bossi, N., and Bossi, L. (2018). Sponges and predators in the small RNA world. Microbiol Spectr *6*, RWR-0021-2018.

Figueroa-Bossi, N., Schwartz, A., Guillemardet, B., D'Heygère, F., Bossi, L., and Boudvillain, M. (2014). RNA remodeling by bacterial global regulator CsrA promotes Rho-dependent transcription termination. Genes Dev *28*, 1239-1251.

Figueroa-Bossi, N., Valentini, M., Malleret, L., Fiorini, F., and Bossi, L. (2009). Caught at its own game: regulatory small RNA inactivated by an inducible transcript mimicking its target. Genes Dev *23*, 2004-2015.

Gall, A.R., Datsenko, K.A., Figueroa-Bossi, N., Bossi, L., Masuda, I., Hou, Y.M., and Csonka, L.N. (2016). Mg^{2+} regulates transcription of *mgtA* in *Salmonella* Typhimurium via translation of proline codons during synthesis of the MgtL peptide. Proc Natl Acad Sci USA *113*, 15096-15101.

Grüll, M.P., and Massé, E. (2019). Mimicry, deception and competition: The life of competing endogenous RNAs. Wiley Interdiscip Rev RNA *10*, e1525.

Guillier, M., and Gottesman, S. (2006). Remodelling of the *Escherichia coli* outer membrane by two small regulatory RNAs. Mol Microbiol *59*, 231-247.

Hemm, M.R., Paul, B.J., Schneider, T.D., Storz, G., and Rudd, K.E. (2008). Small membrane proteins found by comparative genomics and ribosome binding site models. Mol Microbiol *70*, 1487-1501.

Herrero del Valle, A., Seip, B., Cervera-Marzal, I., Sacheau, G., Seefeldt, A.C., and Innis, C.A. (2020). Ornitine capture by a translating ribosome controls bacterial polyamine synthesis. Nat Microbiol *5*, 554-561.

Higashi, K., Ishigure, H., Demizu, R., Uemura, T., Nishino, K., Yamaguchi, A., Kashiwagi, K., and Igarashi, K. (2008a). Identification of a spermidine excretion protein complex (MdtJI) in *Escherichia coli*. J Bacteriol *190*, 872-878.

Higashi, K., Terui, Y., Suganami, A., Tamura, Y., Nishimura, K., Kashiwagi, K., and Igarashi, K. (2008b). Selective structural change by spermidine in the bulged-out region of double-stranded RNA and its effect on RNA function. J Biol Chem *283*, 32989-32994.

Hobbs, E.C., Astarita, J.L., and Storz, G. (2010). Small RNAs and small proteins involved in resistance to cell envelope stress and acid shock in *Escherichia coli*: analysis of a bar-coded mutant collection. J Bacteriol *192*, 59-67.

Hollands, K., Proshkin, S., Sklyarova, S., Epshtein, V., Mironov, A., Nudler, E., and Groisman, E.A. (2012). Riboswitch control of Rho-dependent transcription termination. Proc Natl Acad Sci USA *109*, 5376-5381.

Hör, J., Matera, G., Vogel, J., Gottesman, S., and Storz, G. (2020). Trans-acting small RNAs and their effects on gene expression in *Escherichia coli* and *Salmonella typhimurium*. EcoSal Plus, ESP-0030-2019.

Iosub, I.A., van Nues, R.W., McKellar, S.W., Nieken, K.J., Marchioretto, M., Sy, B., Tree, J.J., Viero, G., and Granneman, S. (2020). Hfq CLASH uncovers sRNA-target interaction networks linked to nutrient availability adaptation. eLife *9*, e54655.

Johansen, J., Rasmussen, A.A., Overgaard, M., and Valentin-Hansen, P. (2006). Conserved small non-coding RNAs that belong to the sE regulon: role in down-regulation of outer membrane proteins. J Mol Biol *364*, 1-8.

Ju, X., Li, D., and Liu, S. (2019). Full-length RNA profiling reveals pervasive bidirectional transcription terminators in bacteria. Nat Microbiol *4*, 1907-1918.

Kawai, Y., Mercier, R., Wu, L.J., Domínguez-Cuevas, P., Oshima, T., and Errington, J. (2015). Cell growth of wall-free L-form bacteria is limited by oxidative damage. Curr Biol *25*, 1613-1618.

Konan, K.V., and Yanofsky, C. (1997). Regulation of the *Escherichia coli tna* operon: nascent leader peptide control at the *tnaC* stop codon. J Bacteriol *179*, 1774-1779.

Kreuzer, K.D., and Henkin, T.M. (2018). The T-box riboswitch: tRNA as an effector to modulate gene regulation. Microbiol Spectr *6*, RWR-0028-2018.

Kriner, M.A., and Groisman, E.A. (2015). The bacterial transcription termination factor Rho coordinates Mg^{2+} homeostasis with translational signals. J Mol Biol *427*, 3834-3849.

Kriner, M.A., Sevostyanova, A., and Groisman, E.A. (2016). Learning from the leaders: gene tegulation by the transcription termination factor Rho. Trends Biochem Sci *41*, 690-699.

Lalaouna, D., Carrier, M.C., Semsey, S., Brouard, J.S., Wang, J., Wade, J.T., and Massé, E. (2015). A 3' external transcribed spacer in a tRNA transcript acts as a sponge for small RNAs to prevent transcriptional noise. Mol Cell *58*, 393-405.

Landt, S.G., Marinov, G.K., Kundaje, A., Kheradpour, P., Pauli, F., Batzoglou, S., Bernstein, B.E., Bickel, P., Brown, J.B., Cayting, P.*, et al.* (2012). ChIP-seq guidelines and practices of the ENCODE and modENCODE consortia. Genome Res *22*, 1813-1831.

Lawther, R.P., and Hatfield, G.W. (1980). Multivalent translational control of transcription termination at attenuator of *ilvGEDA* operon of *Escherichia coli* K-12. Proc Natl Acad Sci USA *77*, 1862-1866.

Li, H., Handsaker, B., Wysoker, A., Fennell, T., Ruan, J., Homer, N., Marth, G., Abecasis, G., Durbin, R., and Subgroup, G.P.D.P. (2009). The sequence alignment/map format and SAMtools. Bioinformatics *25*, 2078-2079.

Loh, E., Righetti, F., Eichner, H., Twittenhoff, C., and Narberhaus, F. (2018). RNA thermometers in bacterial pathogens. Microbiol Spectr *6*, RWR-0012-2017.

Martin, M. (2011). Cutadapt removes adapter sequences from high-throughput sequencing reads. EMBnetjournal *17*, 10-12.

Martinez, A., Opperman, T., and Richardson, J.P. (1996). Mutational analysis and secondary structure model of the RNP1-like sequence motif of transcription termination factor Rho. J Mol Biol *257*, 895-908.

Melamed, S., Adams, P.P., Zhang, A., Zhang, H., and Storz, G. (2020). RNA-RNA interactomes of ProQ and Hfq reveal overlapping and competing roles. Mol Cell *77*, 411-425.

Melamed, S., Faigenbaum-Romm, R., Peer, A., Reiss, N., Shechter, O., Bar, A., Altuvia, Y., Argaman, L., and Margalit, H. (2018). Mapping the small RNA interactome in bacteria using RIL-seq. Nat Protoc *13*, 1-33.

Melamed, S., Peer, A., Faigenbaum-Romm, R., Gatt, Y.E., Reiss, N., Bar, A., Altuvia, Y., Argaman, L., and Margalit, H. (2016). Global Mapping of Small RNA-Target Interactions in Bacteria. Mol Cell *63*, 884-897.

Melior, H., Li, S., Madhugiri, R., Stötzel, M., Azarderakhsh, S., Barth-Weber, S., Baumgardt, K., Ziebuhr, J., and Evguenieva-Hackenberg, E. (2019). Transcription attenuation-derived small RNA rnTrpL regulates tryptophan biosynthesis gene expression in trans. Nucleic Acids Res *47*, 6396-6410.

Mellin, J.R., Koutero, M., Dar, D., Nahori, M.-A., Sorek, R., and Cossart, P. (2014). Riboswitches. sequestration of a two-component response regulator by a riboswitch-regulated noncoding RNA. Science *345*, 940-943.

Mitra, P., Ghosh, G., Hafeezunnisa, M., and Sen, R. (2017). Rho protein: roles and mechanisms. Annu Rev Microbiol *71*, 687-709.

Moon, K., and Gottesman, S. (2009). A PhoQ/P-regulated small RNA regulates sensitivity of *Escherichia coli* to antimicrobial peptides. Mol Microbiol *74*, 1314-1330.

Morita, M., Kanemori, M., Yanagi, H., and Yura, T. (1999a). Heat-induced synthesis of s^{32} in *Escherichia coli*: structural and functional dissection of *rpoH* mRNA secondary structure. J Bacteriol *181*, 401-410.

Morita, M.T., Tanaka, Y., Kodama, T.S., Kyogoku, Y., Yanagi, H., and Yura, T. (1999b). Translational induction of heat shock transcription factor sigma32: evidence for a built-in RNA thermosensor. Genes Dev *13*, 655-665.

Orr, M.W., Mao, Y., Storz, G., and Qian, S.B. (2020). Alternative ORFs and small ORFs: shedding light on the dark proteome. Nucleic Acid Res *48*, 1029-1042.

Overgaard, M., Johansen, J., Møller-Jensen, J., and Valentin-Hansen, P. (2009). Switching off small RNA regulation with trap-mRNA. Mol Microbiol *73*, 790-800.

Ozsolak, F., and Milos, P.M. (2011). Transcriptome profiling using single-molecule direct RNA sequencing. Methods Mol Biol *733*, 51-61.

Peschek, N., Hoyos, M., Herzog, R., Förstner, K.U., and Papenfort, K. (2019). A conserved RNA seed-pairing domain directs small RNA-mediated stress resistance in enterobacteria. EMBO J *38*, e101650.

Peters, J.M., Mooney, R.A., Grass, J.A., Jessen, E.D., Tran, F., and Landick, R. (2012). Rho and NusG suppress pervasive antisense transcription in *Escherichia coli*. Genes Dev *26*, 2621-2633.

Peters, J.M., Mooney, R.A., Kuan, P.F., Rowland, J.L., Keles, S., and Landick, R. (2009). Rho directs widespread termination of intragenic and stable RNA transcription. Proc Natl Acad Sci USA *106*, 15406-154011.

Quinlan, A.R., and Hall, I.M. (2010). BEDTools: a flexible suite of utilities for comparing genomic features. Bioinformatics *26*, 841-842.

Ramírez, F., Ryan, D.P., Grüning, B., Bhardwaj, V., Kilpert, F., Richter, A.S., Heyne, S., Dündar, F., and Manke, T. (2016). deepTools2: a next generation web server for deep-sequencing data analysis Nucleic Acid Res *44*, W160–W165.

Regulski, E.E., Moy, R.H., Weinberg, Z., Barrick, J.E., Yao, Z., Ruzzo, W.L., and Breaker, R.R. (2008). A widespread riboswitch candidate that controls bacterial genes involved in molybdenum cofactor and tungsten cofactor metabolism. Mol Microbiol *68*, 918-932.

Reppas, N.B., Wade, J.T., Church, G.M., and Struhl, K. (2006). The transition between transcriptional initiation and elongation in *E. coli* is highly variable and often rate limiting. Mol Cell *24*, 747-757.

Roberts, J.W. (2019). Mechanisms of bacterial transcription termination. J Mol Biol *431*, 4030-4039.

Romeo, T., and Babitzke, P. (2019). Global regulation by CsrA and its RNA antagonists. Microbiol Spectr *6*, RWR-0009-2017.

Schu, D.J., Zhang, A., Gottesman, S., and Storz, G. (2015). Alternative Hfq-sRNA interaction modes dictate alternative mRNA recognition. EMBO J *34*, 2557-2573.

Sedlyarova, N., Shamovsky, I., Bharati, B.K., Epshtein, V., Chen, J., Gottesman, S., Schroeder, R., and Nudler, E. (2016). sRNA-mediated control of transcription termination in *E. coli*. Cell *167*, 111-121.

Sherlock, M.E., Malkowski, S.N., and Breaker, R.R. (2017). Biochemical validation of a second guanidine riboswitch class in bacteria. Biochemistry *56*, 352-358.

Shishkin, A.A., Giannoukos, G., Kucukural, A., Ciulla, D., Busby, M., Surka, C., Chen, J., Bhattacharyya, R.P., Rudy, R.F., Patel, M.M.*, et al.* (2015). Simultaneous generation of many RNA-seq libraries in a single reaction. Nat Methods *12*, 323-325.

Smirnov, A., Förstner, K.U., Holmqvist, E., Otto, A., Günster, R., Becher, D., Reinhardt, R., and Vogel, J. (2016). Grad-seq guides the discovery of ProQ as a major small RNA-binding protein. Proc Natl Acad Sci USA *113*, 11591-11596.

Storz, G., Vogel, J., and Wassarman, K.M. (2011). Regulation by small RNAs in bacteria: expanding frontiers. Mol Cell *43*, 880-891.

Stringer, A.M., Currenti, S., Bonocora, R.P., Baranowski, C., Petrone, B.L., Palumbo, M.J., Reilly, A.A., Zhang, Z., Erill, I., and Wade, J.T. (2014). Genome-scale analyses of *Escherichia coli* and *Salmonella enterica* AraC reveal noncanonical targets and an expanded core regulon. J Bacteriol *196*, 660-671.

Stringer, A.M., Singh, N., Yermakova, A., Petrone, B.L., Amarasinghe, J.J., Reyes-Diaz, L., Mantis, N.J., and Wade, J.T. (2012). FRUIT, a scar-free system for targeted chromosomal mutagenesis, epitope tagging, and promoter replacement in *Escherichia coli* and *Salmonella enterica*. PLoS One *7*, e44841.

Thomason, M.K., Bischler, T., Eisenbart, S.K., Forstner, K.U., Zhang, A., Herbig, A., Nieselt, K., Sharma, C.M., and Storz, G. (2015). Global transcriptional start site mapping using differential RNA sequencing reveals novel antisense RNAs in *Escherichia coli.* J Bacteriol *197*, 18-28.

Udekwu, K.I., Darfeuille, F., Vogel, J., Reimegård, J., Holmqvist, E., and Wagner, E.G.H. (2005). Hfq-dependent regulation of OmpA synthesis is mediated by an antisense RNA. Genes Dev *19*, 2355-2366.

VanOrsdel, C.E., Kelly, J.P., Burke, B.N., Lein, C.D., Oufiero, C.E., Sanchez, J.F., Wimmers, L.E., Hearn, D.J., Abuikhdair, F.J., Barnhart, K.R*., et al.* (2018). Identifying new small proteins in *Escherichia coli*. Proteomics *18*, e1700064.

Wang, X., N, M.P.A., Jeon, H.J., Lee, Y., He, J., Adhya, S., and Lim, H.M. (2019). Processing generates 3' ends of RNA masking transcription termination events in prokaryotes. Proc Natl Acad Sci USA *116*, 4440-4445.

Weaver, J., Mohammad, F., Buskirk, A.R., and Storz, G. (2019). Identifying small proteins by ribosome profiling with stalled initiation complexes. mBio *10*, e02819-02818.

Weiss, D.S., Pogliano, K., Carson, M., Guzman, L.M., Fraipont, C., Nguyen-Distèche, M., Losick, R., and Beckwith, J. (1997). Localization of the *Escherichia coli* cell division protein Ftsl (PBP3) to the division site and cell pole. Mol Microbiol *25*, 671-681.

Yan, B., Boitano, M., Clark, T.A., and Ettwiller, L. (2018). SMRT-Cappable-seq reveals complex operon variants in bacteria. Nat Commun *9*, 3676.

Yohannes, E., Thurber, A.E., Wilks, J.C., Tate, D.P., and Slonczewski, J.L. (2005). Polyamine stress at high pH in *Escherichia coli* K-12. BMC Microbiol *5*, 59.

Yoshida, M., Meksuriyen, D., Kashiwagi, K., Kawai, G., and Igarashi, K. (1999). Polyamine stimulation of the synthesis of oligopeptide-binding protein (OppA). Involvement of a structural change of the Shine-Dalgarno sequence and the initiation codon AUG in *oppA* mRNA. J Biol Chem *274*, 22723-22728.

Yu, D., Ellis, H.M., Lee, E.C., Jenkins, N.A., Copeland, N.G., and Court, D.L. (2000). An efficient recombination system for chromosome engineering in *Escherichia coli*. Proc Natl Acad Sci USA *97*, 5978-5983.

Zengel, J.M., and Lindahl, L. (1994). Diverse mechanisms for regulating ribosomal protein synthesis in *Escherichia coli*. Prog Nucleic Acid Res Mol Biol *47*, 331–370.

Zhang, A., Wassarman, K.M., Ortega, J., Steven, A.C., and Storz, G. (2002). The Sm-like Hfq protein increases OxyS RNA interaction with target mRNAs. Mol Cell *9*, 11-22.

FIGURE LEGENDS

Figure 1. Distribution of 3′ ends and putative sites of Rho termination

(A) Schematic of classification of Term-seq 3′ ends and Rho termination sites relative to an annotated ORF. 3′ ends and termination sites were defined as: primary (purple colored, located on the same strand within 50 bp downstream of the 3′ end of an annotated gene (mRNA ORF, tRNA, rRNA or sRNA)), antisense (aquamarine colored, located on the opposite strand within 50 bp of a gene start and end coordinates), internal (green-slate colored, located on the same strand within a gene) and orphan (fuchsia colored, located in a 5′ UTR, long 3′ UTR or not falling in any of the previous classes). The black arrow is representative of an ORF.

(B) Distribution of Term-seq 3′ ends relative to annotated genes.

(C) Distribution of Rho termination sites relative to annotated genes based on DirectRNA-seq after BCM treatment.

(D) C:G ratio of sequences surrounding predicted Rho termination sites. Nucleotide proportions were calculated by scanning 800 nt upstream and downstream Rho 3′ ends (Table S2) using 25 nt windows. Plotted values represent the average ratios for all 412 regions (blue). Control plot (grey) represents average C:G ratios calculated in the same manner for 412 random *E. coli* MG1655 genomic positions.

Figure 2. Experimental validation of premature Rho termination

(A) RNA-seq screenshot of the *sugE* locus displaying sequencing reads from LB 0.4 total RNA-seq, LB 0.4 Term-seq and DirectRNA-seq ±BCM treatment. Total and Term-seq tracks represent an overlay of two biological replicates. Read count ranges are shown in the top of each frame.

The chromosome nucleotide coordinates, relative orientation of the *sugE* and *blc* ORFs (wide black arrows), dominant 3′ end in the *sugE* 5′ UTR from Table S3 (small black arrow labeled 3′ end), and *sugE* TSS (Thomason et al., 2015) (bent green arrow) are indicated.

(B) RNA-seq screenshot of the *mdtJI* locus, labeled as in panel A.

(C) RNA-seq screenshot of the *ispU* locus, labeled as in panel A.

(D) β-galactosidase activity for *sugE*, *cfa*, *cyaA*, *mdtJ*, *eptB* and *ispU* 5′ UTR + ORF transcriptional fusions to *lacZ* in WT (AMD054) and *rhoR66S* mutant (GB4). All gene-reporter fusions initiate from the same high expression promoter and were assayed at OD_{600} ~0.4-0.6 (see Materials and Methods for details). Values represent the mean of at least three independent replicates (indicated by black dots). Error bars represent one standard deviation from the mean. The *rhoR66S* vs WT fold change is reported above the values for each 5′ UTR. A *speA* 5′ UTR + ORF-*lacZ* could not be assayed because cells did not grow, likely because of toxicity associated with overexpression of the full-length gene product.

(E) β-galactosidase activity for *sugE*, *cfa*, *cyaA*, *speA*, *mdtJ*, *eptB* and *ispU* 5′ UTR transcriptional fusions to *lacZ* in WT (AMD054) and *rhoR66S* mutant (GB4). Experiments were performed and data analyzed as in panel D. DirectRNA-seq Rho scores for the dominant 3′ end in the 5′ UTR (from Table S3) of these loci are: 1.8 for *sugE*, 2.2 for *cfa*, 2.9 for *cyaA*, 2.6 for *speA*, 2.1 for *mdtJ*, 1.8 for *eptB* and 0.8 for *ispU*.

(F) Northern analysis for *sugE*, *cfa*, *cyaA*, *speA*, *mdtJ*, *eptB* and *ispU* 5′ UTRs in WT (GSO989) and *rhoR66S* mutant (GSO990) cells. Cells were grown to OD_{600} ~0.4 or 2.0 after a dilution of the overnight culture (OD_{600} = 0.05) and lysed. Total RNA was extracted, separated on an acrylamide gel, transferred to a membrane and probed for the indicated RNAs (RNAs were probed sequentially on the same membrane). Blot was also probed for 5S (Figure S2C). Size

markers are indicated for all RNAs. Asterisks signify the transcript predicted to correlate to the 3′ end in Table S3.

Figure 3. Effect of spermidine on *mdtJI* expression

(A) Sequence of the *mdtJI* 5′ UTR. The transcription start site (green shaded nucleotide) determined by dRNA-seq (Thomason et al., 2015) and 3′ end (red shaded nucleotide) determined by Term-seq (current study) are indicated. Sequence encoding the *mdtU* uORF is highlighted in gray. Start codon of the *mdtJ* ORF is indicated with green text.

(B) Northern analysis of effects of spermidine on *mdtJI* mRNA levels. WT (GSO989) cells were grown for 150 min after a dilution of the overnight culture (OD_{600} = 0.05), ±10 mM spermidine in either LB pH 6.9 or LB pH 9.0. Total RNA was extracted, separated on an agarose gel, transferred to a membrane and sequentially probed for the *mdtJI* 5′ UTR and 5S.

(C) β-galactosidase activity of a *mdtU* translational *lacZ* fusion. WT *mdtU* (pASW1) and start codon (ATG→ACG) mutant (pGB337) were assayed and analyzed as in Figure 2D. Constructs included the native *mdtUJI* TSS and full-length *mdtU* ORF.

(D) Northern and western analyses of *mdtU* uORF mutant on *mdtJ*-3XFLAG-*mdtI* mRNA and MdtJ-3XFLAG levels. WT *mdtU* (GSO991) and start codon (ATG→ACG) mutant (GSO992) cells harboring an *mdtJ*-3XFLAG were grown for 150 min after a dilution of the overnight culture (OD_{600} = 0.05), ±10 mM spermidine in LB pH 9.0. Total RNA was analyzed as in panel B. Protein extracts were separated on a Tris-Glycine gel, transferred to a membrane, stained using Ponceau S stain, and probed using α-FLAG antibodies. We do not know the identity of the higher molecular weight bands observed for the WT sample in the western analysis.

(E) Northern analysis of Rho effect on *mdtJI* mRNA levels in the presence of spermidine. WT (GSO989) and *rhoR66S* mutant (GSO990) cells were grown for 150 min after a dilution of the overnight culture (OD_{600} = 0.05), ±10 mM spermidine in LB pH 9.0. Total RNA was analyzed as in panel B.

Figure 4. Effect of sRNA deletions on *eptB*, *ompA* and *chiP* fragments

(A) Sequence of documented region of sRNA-mRNA pairing. 3′ end determined by Term-seq is highlighted in red. Start codon of the corresponding ORF is indicated with green text.

(B) Northern analysis of *eptB*, *ompA*, and *chiPQ* mRNAs. WT (GSO982) with indicated plasmids and Δ*mgrR* (GSO993), Δ*micA* (GSO994), and Δ*chiX* (GSO995) cells were grown for 150 min after a dilution of the overnight culture (OD_{600} = 0.05). Total RNA was extracted, separated on an agarose gel, transferred to a membrane and sequentially probed for specific mRNAs and 5S. Size markers are indicated for all RNAs.

(C) Northern analysis of *eptB*, *ompA*, and *chiP* 5′ UTR fragments. The same RNA from panel B was separated on an acrylamide gel, transferred to a membrane and probed for specific 5′ UTR fragments and 5S. Size markers are indicated for all RNAs.

Figure 5. 5′ UTR-derived sRNAs ChiZ and IspZ act as sRNA sponges

(A) Northern analysis for ChiZ in WT (GSO989) and *rhoR66S* mutant (GSO990) cells. Cells were grown to OD_{600} ~0.4 or 2.0 after a dilution of the overnight culture (OD_{600} = 0.05). Total RNA was extracted, separated on an acrylamide gel, transferred to a membrane and probed for ChiZ and 5S. This is the same blot depicted in Figure 2F and S2C.

(B) Northern analysis of ChiZ effect on *chiP* mRNA. RNA was extracted from WT (GSO982) and Δ*hfq* (GSO955) cells at 150 min after dilution of the overnight culture (OD_{600} = 0.05). Total RNA was separated on an acrylamide or agarose gel, transferred to a membrane and probed for the indicated RNAs (RNAs were probed sequentially on the same membrane).

(C) β-galactosidase activity for *chiP* translational fusions to *lacZ* in WT (PA258) and Δ*chiX* (PA259) strains. Cells were grown and assayed 150 min after dilution of the overnight culture (OD_{600} = 0.05) (see Materials and Methods for details). Values represent the mean of three independent replicates (indicated by black dots). Error bars represent one standard deviation from the mean.

(D) Model of ChiZ effects on ChiX, with indirect effects on the *chiP* mRNA. ChiZ (derived from the 5′ end of *chiP*) is blue and ChiX is red.

(E) Northern analysis of IspZ effect on OxyS upon oxidative stress. WT (GSO982) and Δ*hfq* (GSO955) cells were grown for 150 min after dilution of the overnight culture (OD_{600} = 0.05) and WT (-H_2O_2) samples were collected. To induce OxyS, 0.2 mM H_2O_2 was spiked into the cultures for 20 min and WT and Δ*hfq* samples were collected. Total RNA was extracted and separated on an acrylamide gel, transferred to a membrane and probed for the indicated RNAs (RNAs were probed sequentially on the same membrane).

(F) Predicted base pairing between IspZ and OxyS with mutations assayed.

(G) Test of direct interaction between IspZ and OxyS. RNA was extracted from WT (GSO982) and *oxyS*-M1 (GSO996) cells transformed with the pBR plasmids at 150 min after dilution of the overnight culture (OD_{600} = 0.05) and 20 min incubation with 0.2 mM H_2O_2. Northern analysis was performed on total RNA as in panel E.

Figure 6. Detection of ORF-internal sRNAs

(A) RNA-seq screenshots of the *ftsI*, *aceK*, *rlmD*, *mglC*, and *ampG* mRNAs containing putative internal sRNAs. Sequencing reads from the LB 0.4 dRNA-seq ((Thomason et al., 2015), HS2 samples), total RNA-seq and Term-seq are displayed. Total RNA-seq and Term-seq tracks represent an overlay of two biological replicates. Read count ranges are shown in the top of each frame. The chromosome nucleotide coordinates, relative orientation of ORFs (wide black arrows), dominant 3′ end from Table S3 (small black arrows labeled 3′ ends), and TSS (green bent arrows) or 5′ processed end (small black arrow labeled 5′ ends) as determined by the ratio of reads between ±TEX tracks, are indicated.

(B) Northern analysis of ORF-internal sRNAs. Left: the same WT (GSO988) RNA samples used for total RNA-seq and Term-seq (panel A). Right: RNA was extracted from WT (GSO982) and Δ*hfq* (GSO954) cells at specific times after dilution of the overnight culture (OD_{600} = 0.05), (60, 150, 210, and 360 min) corresponding to early, middle, and late exponential and stationary phase. Specific times, rather than same OD_{600}, are used because the Δ*hfq* strain reaches a lower final OD_{600}, yet exhibits a similar pattern of growth (Melamed et al., 2020). Total RNA was separated on an acrylamide gel, transferred to a membrane and probed for the indicated RNAs (RNAs were probed sequentially on the same membrane). Size markers are indicated for all RNAs (the region of the northern below 100 nt is shown for *ampG* int).

Figure 7. ORF-internal sRNA FtsO acts as a sponge of the RybB sRNA

(A) RIL-seq screenshot showing RybB chimeras at the *ftsO* locus. Data are from Hfq-FLAG LB RIL-seq performed 150 min after a dilution of the overnight culture (OD_{600} = 0.05), ((Melamed et al., 2020), RIL-seq experiment 2). Top: signals for total RNA (dark gray) and Hfq RIL-seq

single fragments with two biological repeats are overlaid (light gray). Read count ranges are shown in the upper left of each frame. Bottom: chimeras with FtsO, blue lines indicate RybB is the second RNA in the chimera.

(B) RybB and CpxQ levels decrease in the presence of FtsO. RNA was extracted from WT (GSO982) and Δ*hfq* (GSO954) cells at 150 and 360 min after dilution of the overnight culture (OD_{600} = 0.05). Total RNA was separated on an acrylamide gel, transferred to a membrane and probed for the indicated RNAs (RNAs were probed sequentially on the same membrane).

(C) Predicted base pairing between FtsO and RybB with mutations assayed.

(D) Test of direct interaction between FtsO and RybB. RNA was extracted from WT (GSO982) and *rybB*-M3 (GSO997) cells transformed with the pBR plasmids at 360 min after dilution of the overnight culture (OD_{600} = 0.05). Northern analysis was performed on total RNA as in panel B.

(E) Chromosomally-encoded FtsO mutant dysregulates RybB levels under membrane stress. WT tet^R (GSO998) and *ftsO*-M3 tet^R (GSO999) cells were grown for 120 min after dilution of the overnight culture (OD_{600} = 0.05) prior to the addition of EtOH to a final concentration of 5%. Cells were collected and extracted for RNA at the indicated time points after addition of EtOH. Northern analysis was performed on total RNA separated on either acrylamide or agarose gels as in Figure 4B and 4C.

(F) Model showing how same DNA sequence can encode two different gene products. The *ftsI* mRNA encodes the essential FtsI protein, found in the inner membrane (IM). This transcript also encodes the FtsO sRNA (blue), which blocks the activity of the RybB sRNA (red), induced by cell envelope stress, to down regulate the synthesis of outer membrane (OM) porins such as OmpC.

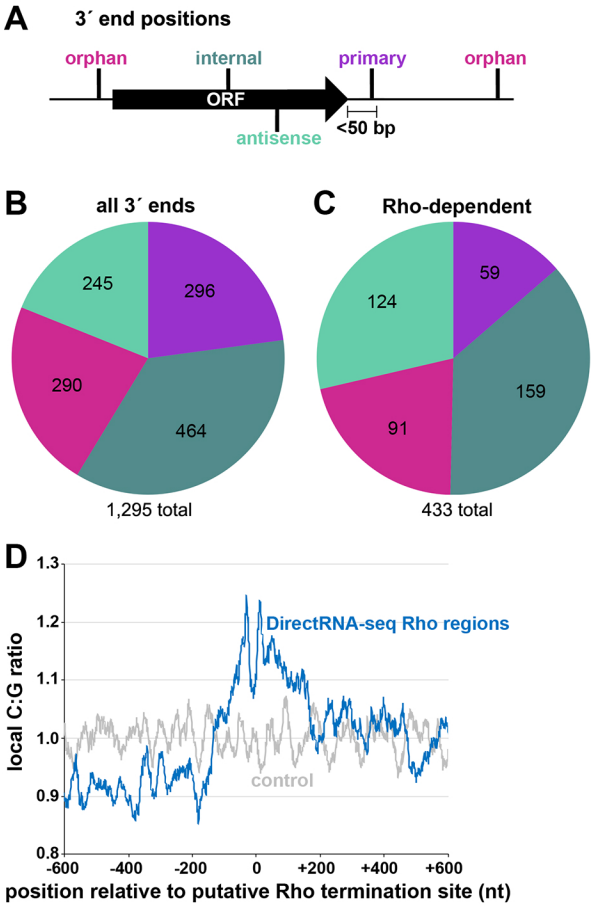
A
3´ end positions
orphan
internal
primary
orphan
ORF
antisense
<50 bp
B
all 3´ ends
245
296
290
464
1,295 total
C
Rho-dependent
124
59
91
159
433 total
D
local C:G ratio
1.3
1.2
1.1
1.0
0.9
0.8
DirectRNA-seq Rho regions
control
-600
-400
-200
0
+200
+400
+600
position relative to putative Rho termination site (nt)

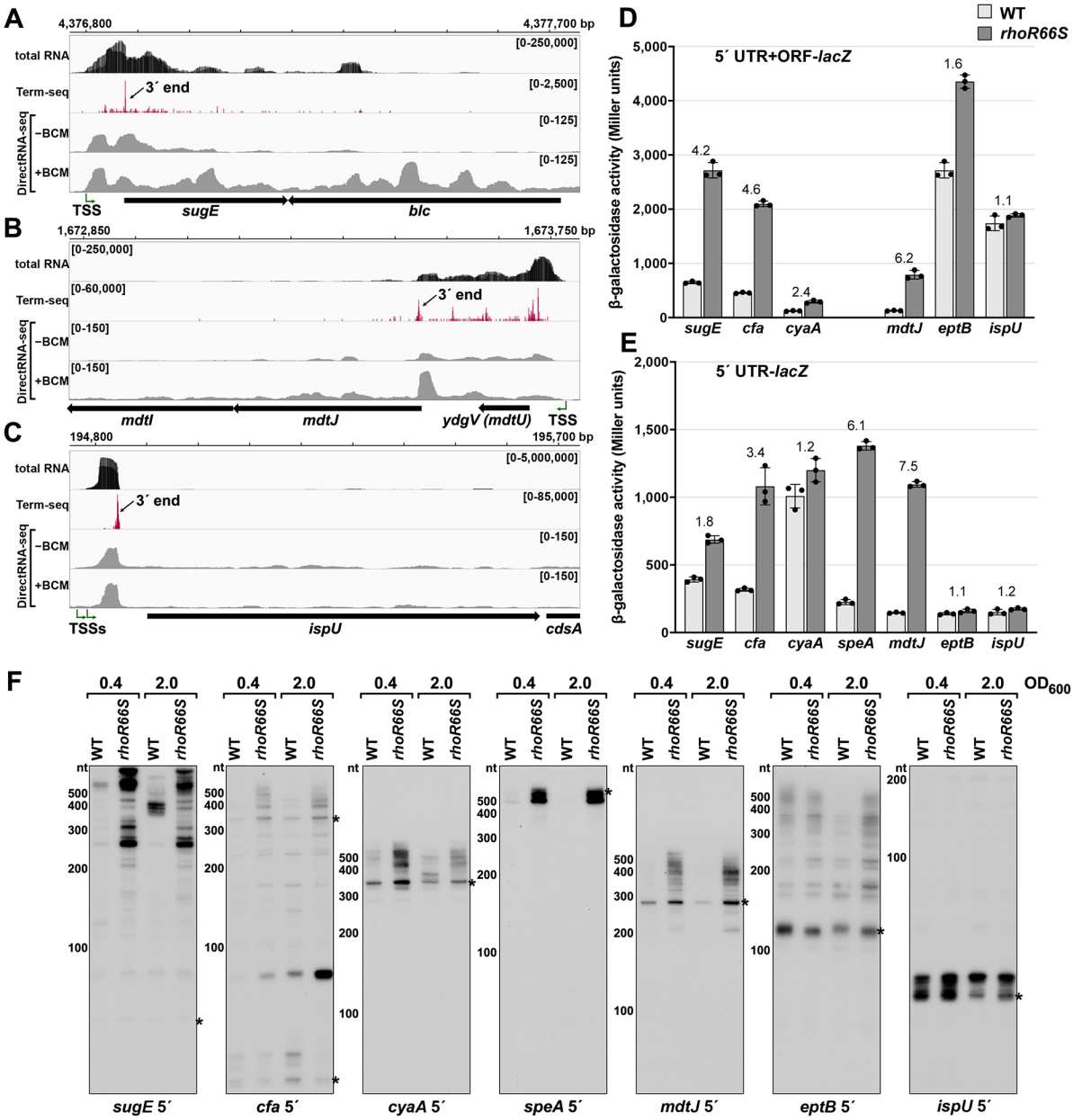
A
4,376,800
4,377,700 bp
total RNA
[0-250,000]
Term-seq
3´ end
[0-2,500]
DirectRNA-seq
−BCM
[0-125]
+BCM
[0-125]
TSS
sugE
blc
B
1,672,850
1,673,750 bp
total RNA
[0-250,000]
Term-seq
[0-60,000]
3´ end
DirectRNA-seq
−BCM
[0-150]
+BCM
[0-150]
mdtI
mdtJ
ydgV (mdtU)
TSS
C
194,800
195,700 bp
total RNA
[0-5,000,000]
Term-seq
3´ end
[0-85,000]
DirectRNA-seq
−BCM
[0-150]
+BCM
[0-150]
TSSs
ispU
cdsA
D
WT
rhoR66S
5´ UTR+ORF-lacZ
β-galactosidase activity (Miller units)
5,000
4,000
3,000
2,000
1,000
0
4.2
4.6
2.4
6.2
1.6
1.1
sugE
cfa
cyaA
mdtJ
eptB
ispU
E
5´ UTR-lacZ
β-galactosidase activity (Miller units)
2,000
1,500
1,000
500
0
1.8
3.4
1.2
6.1
7.5
1.1
1.2
sugE
cfa
cyaA
speA
mdtJ
eptB
ispU
F
0.4
2.0
OD600
WT
rhoR66S
nt
500
400
300
200
100
sugE 5´
cfa 5´
cyaA 5´
speA 5´
mdtJ 5´
eptB 5´
ispU 5´

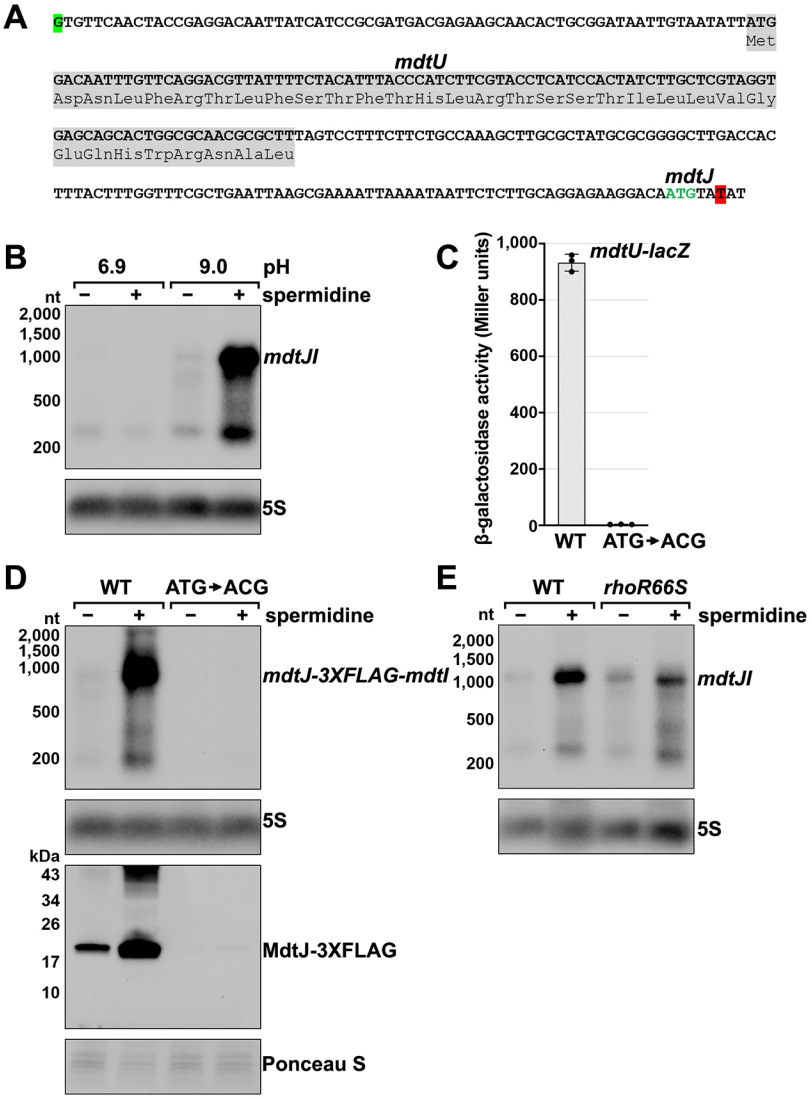
A
GTGTTCAACTACCGAGGACAATTATCATCCGCGATGACGAGAAGCAACACTGCGGATAATTGTAATATTATG
Met
mdtU
GACAATTTGTTCAGGACGTTATTTTCTACATTTACCCATCTTCGTACCTCATCCACTATCTTGCTCGTAGGT
AspAsnLeuPheArgThrLeuPheSerThrPheThrHisLeuArgThrSerSerThrIleLeuLeuValGly
GAGCAGCACTGGCGCAACGCGCTTTAGTCCTTTCTTCTGCCAAAGCTTGCGCTATGCGCGGGGCTTGACCAC
GluGlnHisTrpArgAsnAlaLeu
mdtJ
TTTACTTTGGTTTCGCTGAATTAAGCGAAAATTAAAATAATTCTCTTGCAGGAGAAGGACAATGTATTAT
B
6.9
9.0
pH
nt
–
+
–
+
spermidine
2,000
1,500
1,000
500
200
mdtJI
5S
C
mdtU-lacZ
β-galactosidase activity (Miller units)
1,000
800
600
400
200
0
WT
ATG→ACG
D
WT
ATG→ACG
nt
–
+
–
+
spermidine
2,000
1,500
1,000
500
200
mdtJ-3XFLAG-mdtI
5S
kDa
43
34
26
17
10
MdtJ-3XFLAG
Ponceau S
E
WT
rhoR66S
nt
–
+
–
+
spermidine
2,000
1,500
1,000
500
200
mdtJI
5S

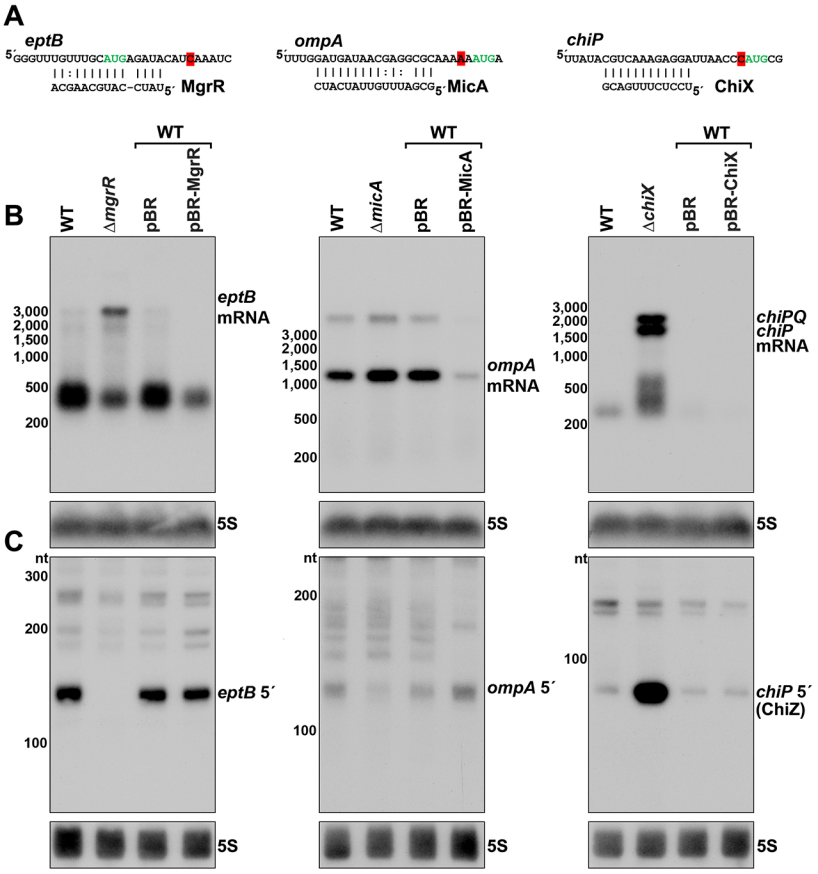
A
eptB
5´GGGUUUGUUUGCAUGAGAUACAUCAAAUC
ACGAACGUAC-CUAU5´ MgrR
ompA
5´UUUGGAUGAUAACGAGGCGCAAAAAUGA
CUACUAUUGUUUAGCG5´ MicA
chiP
5´UUAUACGUCAAAGAGGAUUAACCCAUGCG
GCAGUUUCUCCU5´ ChiX
B
WT
ΔmgrR
pBR
pBR-MgrR
eptB mRNA
3,000
2,000
1,500
1,000
500
200
ΔmicA
pBR-MicA
ompA mRNA
ΔchiX
pBR-ChiX
chiPQ
chiP
mRNA
5S
C
nt
300
200
100
eptB 5´
ompA 5´
chiP 5´
(ChiZ)

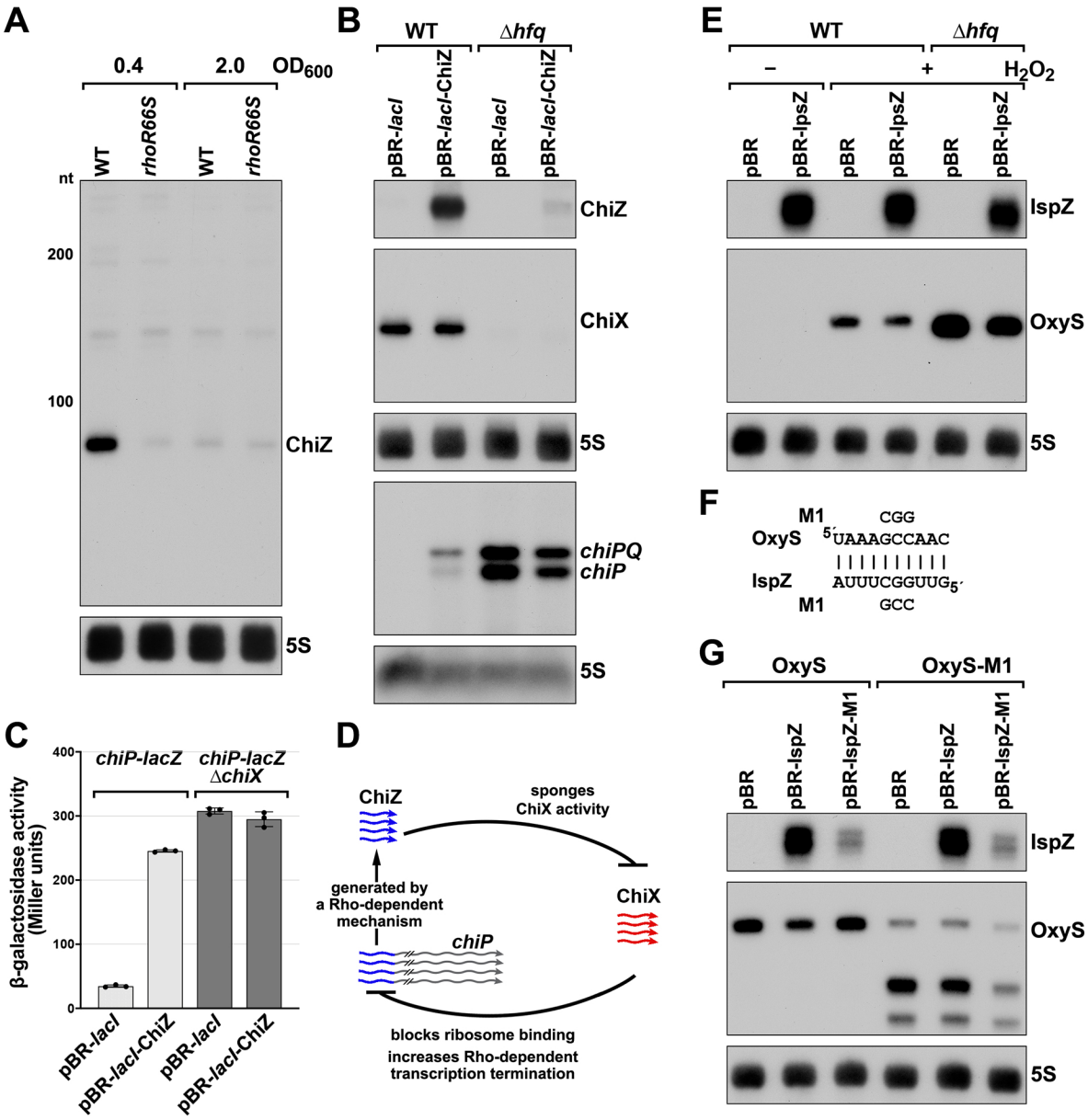
A
0.4
2.0
OD600
WT
rhoR66S
WT
rhoR66S
nt
200
100
ChiZ
5S
B
WT
Δhfq
pBR-lacI
pBR-lacI-ChiZ
pBR-lacI
pBR-lacI-ChiZ
ChiZ
ChiX
5S
chiPQ
chiP
5S
C
chiP-lacZ
chiP-lacZ ΔchiX
β-galactosidase activity (Miller units)
400
300
200
100
0
pBR-lacI
pBR-lacI-ChiZ
pBR-lacI
pBR-lacI-ChiZ
D
ChiZ
sponges ChiX activity
generated by a Rho-dependent mechanism
ChiX
chiP
blocks ribosome binding
increases Rho-dependent transcription termination
E
WT
Δhfq
–
+
H2O2
pBR
pBR-IpsZ
pBR
pBR-IpsZ
pBR
pBR-IpsZ
IspZ
OxyS
5S
F
M1
CGG
OxyS
5′UAAAGCCAAC
IspZ
AUUUCGGUUG5′
M1
GCC
G
OxyS
OxyS-M1
pBR
pBR-IspZ
pBR-IspZ-M1
pBR
pBR-IspZ
pBR-IspZ-M1
IspZ
OxyS
5S

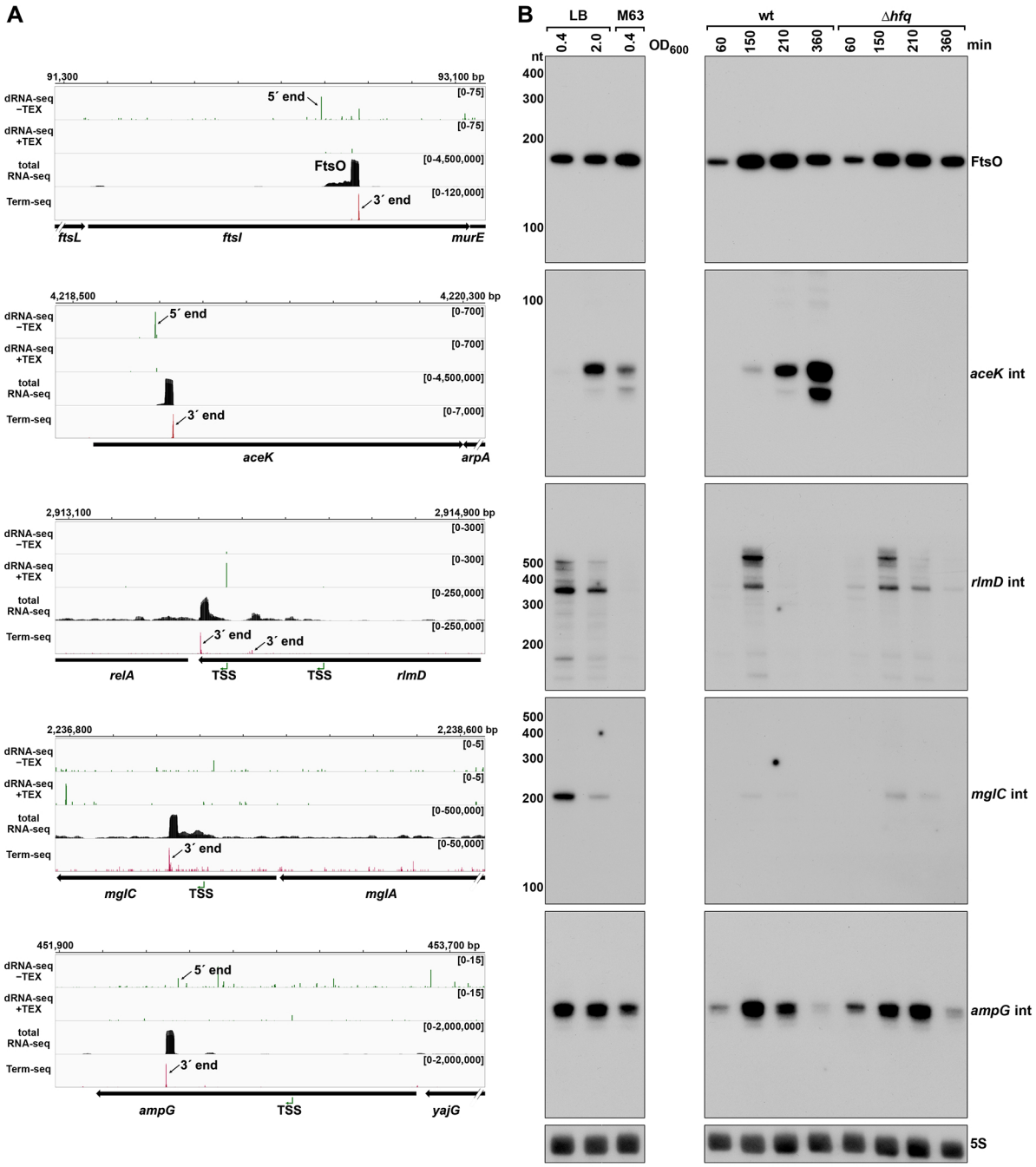
A
91,300
93,100 bp
dRNA-seq −TEX
dRNA-seq +TEX
total RNA-seq
Term-seq
5´ end
FtsO
3´ end
[0-75]
[0-75]
[0-4,500,000]
[0-120,000]
ftsL
ftsI
murE
4,218,500
4,220,300 bp
5´ end
3´ end
[0-700]
[0-700]
[0-4,500,000]
[0-7,000]
aceK
arpA
2,913,100
2,914,900 bp
3´ end
3´ end
[0-300]
[0-300]
[0-250,000]
[0-250,000]
relA
TSS
TSS
rlmD
2,236,800
2,238,600 bp
3´ end
[0-5]
[0-5]
[0-500,000]
[0-50,000]
mglC
TSS
mglA
451,900
453,700 bp
5´ end
3´ end
[0-15]
[0-15]
[0-2,000,000]
[0-2,000,000]
ampG
TSS
yajG
B
LB
M63
wt
Δhfq
0.4
2.0
0.4
OD600
60
150
210
360
60
150
210
360
min
nt
400
300
200
100
FtsO
aceK int
500
400
300
200
rlmD int
mglC int
ampG int
5S

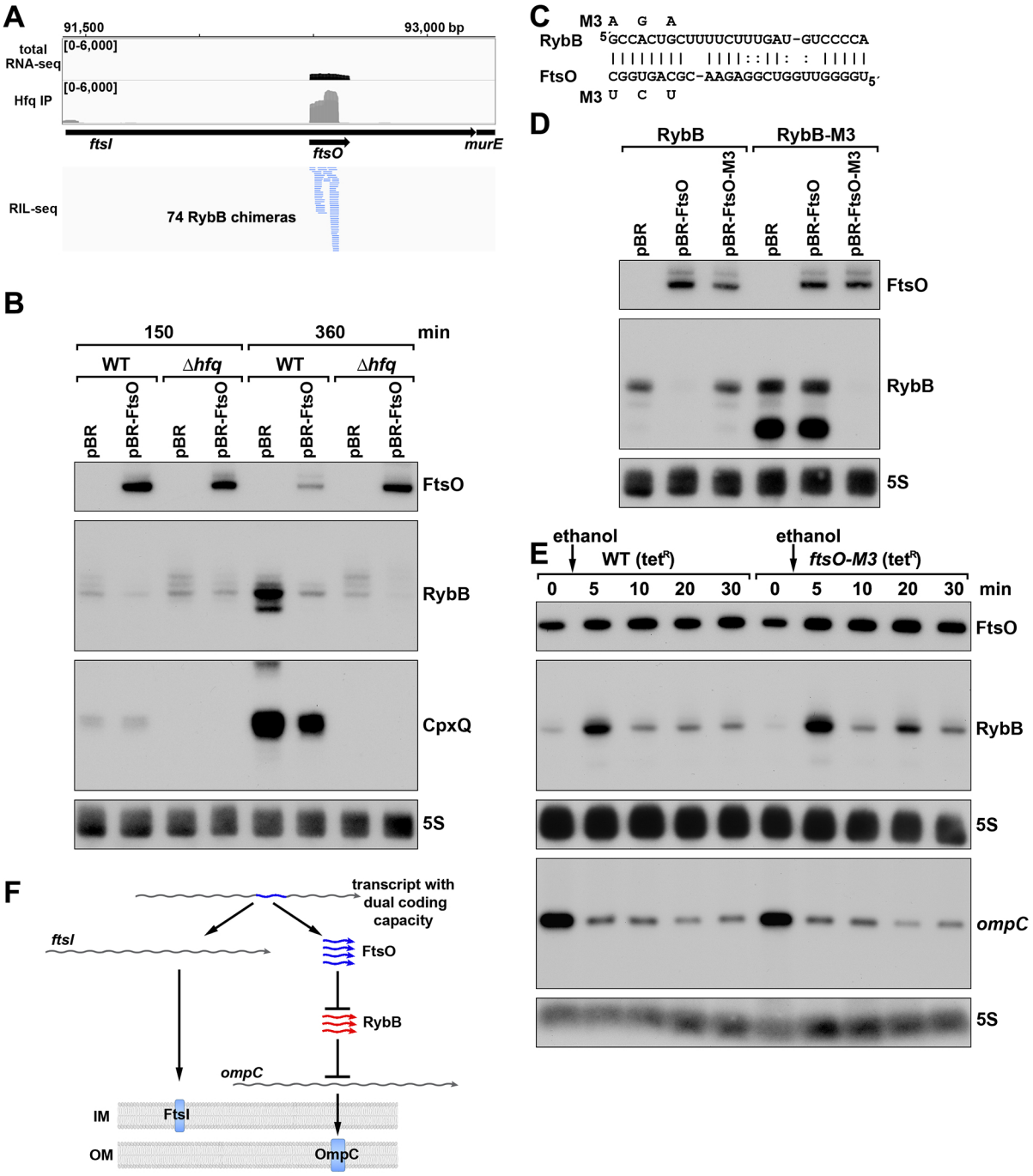
A
91,500
93,000 bp
total RNA-seq
[0-6,000]
Hfq IP
[0-6,000]
ftsI
ftsO
murE
RIL-seq
74 RybB chimeras
B
150
360
min
WT
Δhfq
WT
Δhfq
pBR
pBR-FtsO
pBR
pBR-FtsO
pBR
pBR-FtsO
pBR
pBR-FtsO
FtsO
RybB
CpxQ
5S
C
M3 A G A
RybB 5'GCCACUGCUUUUCUUUGAU-GUCCCCA
FtsO CGGUGACGC-AAGAGGCUGGUUGGGGU5'
M3 U C U
D
RybB
RybB-M3
pBR
pBR-FtsO
pBR-FtsO-M3
pBR
pBR-FtsO
pBR-FtsO-M3
FtsO
RybB
5S
E
ethanol
WT (tetR)
ethanol
ftsO-M3 (tetR)
0 5 10 20 30 0 5 10 20 30 min
FtsO
RybB
5S
ompC
5S
F
transcript with dual coding capacity
ftsI
FtsO
RybB
ompC
IM
FtsI
OM
OmpC